

The Nonlinear Schrödinger Equation in the Finite Line

J. I. Ramos and F. R. Villatoro
Departamento de Lenguajes y Ciencias de la Computación
E. T. S. Ingenieros Industriales
Universidad de Málaga
Plaza El Ejido, s/n
29013-Málaga
SPAIN

Abstract

A numerical study of the nonlinear Schrödinger (NLS) equation subject to homogeneous Dirichlet, Neumann and Robin boundary conditions in the finite line is presented. The results are compared with both the exact analytical ones for the initial-value problem (IVP) of the NLS equation and the numerical ones for periodic boundary conditions. It is shown that initial solutions obtained by truncating the exact N -soliton solution of the IVP of the NLS equation into a finite interval develop solitary waves that behave as solitons, even after collisions with the boundaries. For periodic and homogeneous Dirichlet and Neumann boundary conditions, it is observed that the interaction between solitons and boundaries is equivalent to the collision between solitons in IVP or quarterplane problems. It is shown that for homo-

geneous Robin boundary conditions, boundary layers that trap and delay the soliton are formed at the boundaries. Phase diagrams for the soliton amplitude at the boundary points and for the soliton's maximum amplitude show a recurrent phenomenon, and are similar to those of the cubic Duffing equation. It is also shown that the phase diagrams are strong functions of the parameter that defines the Robin boundary conditions. A method of images, similar to the one used in potential theory, is developed for the NLS equation in the quarter-plane with homogeneous Dirichlet and Neumann boundary conditions at the finite boundary.

KEYWORDS: Nonlinear Schrödinger equation, two-point initial-value problems, phase diagrams, recurrence, nonlinear dynamics

1 Introduction

The NLS equation has been used as a model for the propagation of the envelope of a wave packet in a weakly nonlinear, dispersive medium, and has found many applications in physics, e.g., the propagation of deep water gravity waves in fluid mechanics, the propagation of Langmuir waves in plasma physics and the self-focusing and self-modulation of trains of monochromatic waves in nonlinear optics [1, 2, 3]. Its wide applicability has an analytical justification since the NLS equation emerges from almost all evolution equations characterized by a linear part which is “dispersive” and a nonlinear part which is “analytical” when the interest lies in the modulation of a carrier wave due to weakly nonlinear effects [4]. Furthermore, the NLS equation is

amongst the few nonlinear partial differential equations that have an IVP integrable by the inverse scattering transform [2, 5].

Most of the numerical studies on the NLS equation have been concerned with the IVP or infinite line problem which was truncated to a finite one and subjected to periodic [6, 7, 8], homogeneous Dirichlet [9] or homogeneous Neumann [10, 11, 12] boundary conditions. However, experiments have mainly dealt with the generation of solitons, i.e., boundary-generated solitons, which must be modelled by an initial-boundary value problem in the quarterplane. These initial-boundary value problems for nonlinear integrable systems in the quarterplane are also called ‘forced integrable systems’ [13] because the boundary conditions can be viewed as forces that act at the boundaries.

Despite the great interest that the NLS equation has received in the past two decades through analytical and numerical studies, its initial-boundary value problem in semi-infinite and finite lines is still a subject of current research because of serious analytical difficulties [14]. Three different approaches have been used to study the semi-infinite line, initial-boundary value problem of nonlinear, integrable equations, here referred to as the quarterplane problem, and to analyze the propagation of boundary-generated solitons [15]. The first approach is based on the use of numerical methods to study the soliton’s generation and formation in quarterplane problems subject to nonhomogeneous boundary conditions at the finite boundary. For example, Chu [16] and Chou and Chu [17] studied boundary-generated solitons for the Korteweg-de Vries and Boussinesq equations, respectively. The second approach is based on the inverse scattering transform and employs ad

hoc assumptions in order to model known numerical results. Kaup [13] and Kaup and Hansen [18] used this second approach to study the quarterplane problem of the NLS equation. The third approach is based on extensions of the inverse scattering transform and employs nonlinear sine-Fourier transforms. This approach has been applied to the NLS equation by Ablowitz and Segur [19] who considered homogeneous Dirichlet and Neumann boundary conditions at the finite boundary, and has been generalized by Fokas [20] and Bikbaev and Tarasov [21] for homogeneous Robin boundary conditions. Bikbaev and Tarasov [21] used Bäcklund transformation methods in their analysis, while Fokas [20] has shown that the scattering data for the nonhomogeneous Robin boundary condition problem is governed by a nonlinear, integro-differential equation, although he was unable to obtain its solution. Fokas and Ablowitz [22] have also shown that the infinite-line, forced NLS equation may be used to study the same equation in some quarterplane problems by properly choosing the forcing term.

The initial-boundary value problem of the NLS equation in the finite line has received much less attention than IVP and quarterplane problems. In fact, only the periodic problem seems to have been studied in detail. Ma and Ablowitz [23] have obtained analytically finite N-band potential solutions of the NLS equation subject to periodic boundary conditions by means of the periodic inverse scattering transform. Osborne [24] has developed a fast numerical version of the inverse scattering transform, while Boyd [25] has studied imbricate series and polynoidal waves of the periodic NLS equation. The non-periodic, finite-line, initial-boundary value problem for other integrable, nonlinear evolution equations has also received little attention.

Christiansen [26] and Sirovich et al. [27] have studied numerically the Neumann problem for the sine-Gordon and the Ginzburg-Landau equations, respectively.

In this paper, a numerical study of the initial-boundary value problem of the NLS equation in a finite interval subject to homogeneous Dirichlet, Neumann and Robin boundary conditions at both boundaries is presented. The results are compared with both the exact analytical ones for the IVP of the NLS equation [5] and with the numerical results of the NLS equation subject to periodic boundary conditions. Particular attention is paid to the initial conditions and their mathematical compatibility with the boundary ones, and to the propagation of solitons and their interactions with the boundaries which are compared with those that result from the mutual interactions between solitons in the infinite spatial line, i.e., with those corresponding to the IVP of the NLS equation. It must be noted that collisions between solitons and boundaries have seldom been considered previously, even for other integrable, nonlinear equations except for Christiansen [26] who studied the Neumann boundary-value problem for the sine-Gordon equation in Josephson tunnel junctions, Mirie and Su [28] who analyzed numerically the Neumann boundary-value problem for the Korteweg-de Vries equation, and Chou and Chu [17] who considered the reflection of solitons from a wall for the Boussinesq equation.

The paper has been organized as follows. The one-dimensional NLS equation and its analytical solution for the IVP is presented in Section 2 together with the homogeneous boundary conditions at the ends of the finite line used throughout this paper. The second-order, accurate, finite difference method

employed to solve the NLS equation is described in detail in Section 3. Section 4 is devoted to quarterplane plane problems subject to homogeneous Dirichlet and Neumann at the finite boundary. In that section, it is shown that the collision between a soliton and a homogeneous Neumann boundary condition is equivalent to the collision between two identical solitons of opposite velocities, whereas the collision of a soliton with a homogeneous Dirichlet boundary condition is equivalent to the collision between two solitons of opposite amplitudes and velocities. In Section 4, N -soliton solutions are obtained for the Dirichlet and Neumann quarterplane problems. Section 5 is entirely devoted to the study of the NLS equation in the finite line subject to homogeneous Dirichlet, Neumann, Robin and periodic boundary conditions which are mathematically compatible with the initial conditions. In that section, it is shown that the initial conditions evolve into solitary waves which have a soliton-like shape and retain their shape after collisions with the boundaries except for a phase shift, i.e., they behave as solitons. In Section 5, it is also shown that the collisions of the solitons with the boundaries exhibit a recurrent phenomena which is analyzed by means of phase diagrams for the soliton amplitude at the boundary points and for the soliton maximum amplitude. These diagrams show large topological changes as the parameter that controls the Robin boundary conditions is varied. They also show that the soliton amplitude in both IVP and periodic problems behaves as a nonlinear cubic Duffing equation which may exhibit chaotic behaviour under certain forcings [29].

2 Formulation of the Problem

The one-dimensional NLS equation in dimensionless form can be written as

$$iu_t + u_{xx} + q|u|^2u = 0, \quad x \in \mathcal{D} \text{ and } t \geq 0 \quad (1)$$

where t is time, x is the spatial Cartesian coordinate, u is the complex amplitude, q is a real number, $i = \sqrt{-1}$, the subscripts denote partial differentiation, and \mathcal{D} denotes the domain of definition of the equation, i.e., the whole real line for the IVP, a semi-infinite line with one boundary located at $x=0$, i.e., $\mathcal{D} \equiv [0, \infty)$ for quarterplane problems, or a finite interval, $\mathcal{D} \equiv [-L, L]$, with two boundary conditions for two-point, initial-boundary value problems. Note that, without loss of generality, a symmetric interval has been chosen since the NLS equation is invariant under both translations and mirror reflections in x .

The NLS equation in the infinite line has analytical solutions which can be determined by means of the inverse scattering transform. For example, the exact N -soliton solution of the NLS equation in the infinite line was obtained by Zakharov and Shabat [5]. Gordon [30] essentially reduced by half the number of equations obtained by Zakharov and Shabat and redefined their parameters to give them clearer meanings.

The exact N -soliton solution of the NLS equation given by Gordon [30] can be written as

$$u(x, t) = \frac{1}{\sqrt{q}} \sum_{j=1}^N u_j(x, t), \quad (2)$$

where u_j is the solution of the following system of linear algebraic equations

$$\sum_{k=1}^N M_{jk} u_k = \sum_{k=1}^N \frac{\gamma_j^{-1} + \gamma_k^*}{\lambda_j + \lambda_k^*} u_k = 1, \quad j = 1, 2, \dots, N, \quad (3)$$

and

$$\lambda_j = A_j + iV_j/\sqrt{2}, \quad (4)$$

$$\gamma_j = \exp \left[\lambda_j(x - x_{j0})/\sqrt{2} + i\lambda_j^2 t/2 + i\phi_{j0} \right], \quad (5)$$

where the four real parameters $\{A_j, V_j, x_{j0}, \phi_{j0}\}$ denote the amplitude, velocity, initial location of the maximum amplitude and initial phase, respectively, of the j -th soliton.

Equation (2) can be expanded in the neighborhood of a soliton well separated from the others to yield [30]

$$u_j(x, t) = \frac{A_j}{\sqrt{q}} \operatorname{sech} \left\{ \frac{A_j}{\sqrt{2}}(x - x_j) + \frac{q_j}{\sqrt{2}} \right\} \exp \{ i[\phi_j + \Phi_j] \}, \quad (6)$$

where

$$x_j = x_{j0} + V_j t, \quad \phi_j = \frac{V_j}{2}(x - x_{j0}) + (A_j^2 - \frac{V_j^2}{2})\frac{t}{2} + \phi_{j0}, \quad (7)$$

and the presence of the other distant solitons introduces a displacement, $q_j/\sqrt{2}$, and a phase shift, Φ_j , given by

$$q_j + i\Phi_j = \sum_{k \neq j} \operatorname{sgn}(x_k - x_j) \log \left[\frac{A_j + A_k + i(V_j - V_k)/\sqrt{2}}{A_j - A_k + i(V_j - V_k)/\sqrt{2}} \right], \quad (8)$$

where the sign function, $\operatorname{sgn}(x)$, is equal to one, zero and minus one, for positive, zero and negative x , respectively.

Notice that for the 1-soliton case, Eqs. (2)–(5) yield

$$u(x, t) = \frac{A}{\sqrt{q}} \operatorname{sech} \left\{ \frac{A}{\sqrt{2}}[(x - x_0) - Vt] \right\} \exp \left\{ \frac{i}{2}[V(x - x_0) + (A^2 - \frac{V^2}{2})t] + i\phi_0 \right\}. \quad (9)$$

It is well known that the IVP of the NLS describes a completely integrable Hamiltonian system with the scattering data as action-angle variables and

an infinite set of invariants. The most important invariants of the IVP of the NLS equation are the first, second and third ones. The first, known as wave mass or ‘number of particles’, is

$$I_1 = \int_{-\infty}^{\infty} |u|^2 dx. \quad (10)$$

The second invariant represents the total momentum in the Hamiltonian formalism and is given by

$$I_2 = i \int_{-\infty}^{\infty} (uu_x^* - u^*u_x) dx, \quad (11)$$

where the asterisk denotes complex conjugate. The third invariant is the total energy or Hamiltonian, i.e.,

$$I_3 = \int_{-\infty}^{\infty} \left(|u_x|^2 - \frac{q}{2}|u|^4 \right) dx. \quad (12)$$

It may be easily shown from Eq. (1) that

$$\frac{\partial m}{\partial t} + \frac{\partial M}{\partial x} = 0, \quad (13)$$

where $m = u^*u = |u|^2$ and $M = i(uu_x^* - u^*u_x)$ denote the mass density and linear momentum density, respectively.

In this paper, the analytical solution of the NLS equation in the infinite line is compared with the numerical solution of the same equation in finite lines subject to the following homogeneous, boundary conditions

$$u(x, t) + \gamma u_x(x, t) = 0, \quad x \in \partial\mathcal{D} \text{ and } t \geq 0, \quad (14)$$

where $\gamma=0$ and ∞ correspond to homogeneous Dirichlet and Neumann boundary conditions, respectively, whereas finite values of $\gamma \neq 0$ correspond to homogeneous Robin boundary conditions at both boundaries. In addition, the

NLS equation is also solved in a finite line subject to the following periodic boundary conditions

$$\frac{\partial^n u}{\partial x^n}(x, t) = \frac{\partial^n u}{\partial x^n}(x+2kL, t), \quad \forall n \geq 0, \quad k \in \mathbf{Z}, \quad x \in \mathcal{D} \equiv [-L, L] \quad \text{and} \quad t \geq 0. \quad (15)$$

Hereon, the NLS equation subject to periodic and homogeneous Dirichlet, Neumann and Robin boundary conditions will be referred to as the periodic, Dirichlet, Neumann and Robin problems, respectively.

3 Numerical Scheme Used in the Simulations

For the numerical integration of Eq. (1) in the interval $[-L, L]$, the Crank-Nicolson finite difference method has been used. This method can be written as

$$i \frac{U_j^{n+1} - U_j^n}{\Delta t} + \frac{1}{\Delta x^2} \delta^2 U_j^{n+1/2} + q |U_j^{n+1/2}|^2 U_j^{n+1/2} = 0, \quad (16)$$

where

$$\delta^2 U_j^n = U_{j+1}^n - 2U_j^n + U_{j-1}^n, \quad U_j^{n+1/2} = \frac{U_j^{n+1} + U_j^n}{2},$$

and

$$U_j^n = u(-L + j\Delta x, n\Delta t),$$

$$j = 0, 1, \dots, N, \quad n \geq 1, \quad \Delta x = 2L/N, \quad \Delta t > 0,$$

where $(N+1)$ is the number of grid points; Δx is the spatial step size; and, Δt is the time step. This scheme is second-order accurate in both space and time, i.e., $O(\Delta t^2, \Delta x^2)$.

The discrete boundary conditions are as follows (cf. Eq. (14)). For the Dirichlet boundary conditions, i.e., $\gamma = 0$,

$$U_0^{n+1/2} = U_N^{n+1/2} = 0. \quad (17)$$

For the Neumann boundary conditions, i.e., $\gamma = \infty$,

$$\frac{U_1^{n+1/2} - U_{-1}^{n+1/2}}{2\Delta x} = \frac{U_{N+1}^{n+1/2} - U_{N-1}^{n+1/2}}{2\Delta x} = 0. \quad (18)$$

For the Robin boundary conditions, i.e., $\gamma \neq 0$ and $\gamma \neq \infty$,

$$U_0^{n+1/2} + \gamma \frac{U_1^{n+1/2} - U_{-1}^{n+1/2}}{2\Delta x} = U_N^{n+1/2} + \gamma \frac{U_{N+1}^{n+1/2} - U_{N-1}^{n+1/2}}{2\Delta x} = 0. \quad (19)$$

For the periodic boundary conditions (cf. Eq. (15))

$$U_{N+1}^{n+1/2} = U_1^{n+1/2}, \quad U_{-1}^{n+1/2} = U_{N-1}^{n+1/2}. \quad (20)$$

Note that two fictitious points have been introduced at $j=-1$ and $j=N+1$, except in the Dirichlet problem, in order to preserve the second-order, spatial accuracy of the Crank-Nicolson method.

It can be easily shown that the Crank-Nicolson method is linearly stable and nonlinearly stable by means of an energy method. The existence and convergence of the discrete solutions of the discretized IVP of the NLS equation have been proved by Ben-Yu [31] and his results can be extended to a finite interval with homogeneous boundary conditions.

An iterative, Newton-Raphson method has been used to solve the nonlinear algebraic system of equations (cf. Eq. (16)). The convergence of this method for finite-line problems can be proven using similar methods to those employed by Akrivis [9]. The diagonally dominant, tridiagonal system

of linear algebraic equations that result from the Newton-Raphson method has been solved by a 2×2 block-oriented version of the Thomas algorithm. For periodic problems, a natural optimization of the Gaussian elimination technique for cyclic-tridiagonal systems has been used before employing the Thomas algorithm [8].

The Crank-Nicolson method is conservative since it preserves a discrete equivalent of the mass (cf. Eq. (10)), i.e., the L^2 norm of the solution, for the discrete, infinite line IVP and for finite line problems subject to periodic or homogeneous Dirichlet boundary conditions. For homogeneous Neumann and Robin boundary conditions, the mass is nearly preserved when the solitons are far away from, i.e., they are not affected by, the boundaries or when a small $\Delta t / \Delta x^2$ is employed in the numerical calculations. This can be shown as follows. The imaginary part of the sum (in j) of the product of Eq. (16) times $(U_j^{n+1} + U_j^n)^*$ yields

$$\|U^{n+1}\| = \|U^n\| = \|U^0\|, \quad n \geq 1 \quad (21)$$

for the discrete, infinite line problem and for both the periodic and the Dirichlet problems, and

$$\begin{aligned} \|U^{n+1}\| - \|U^n\| - \frac{\Delta t}{2\Delta x^2} \mathcal{Im}[(U_1^{n+1} + U_1^n)(U_0^{n+1} + U_0^n)^* + \\ + (U_{N-1}^{n+1} + U_{N-1}^n)(U_N^{n+1} + U_N^n)^*] = 0 \end{aligned} \quad (22)$$

for the Neumann and Robin problems, where \mathcal{Im} denotes imaginary part and $\|U_j^n\|$ represents the L^2 norm of U_j^n .

In previous numerical papers, e.g., [6]–[12], only the mass (cf. Eq. (10)) and energy (cf. Eq. (12)) have been studied in order to assess the conservation properties of the numerical methods used to solve the NLS equation in

infinite lines which were truncated to finite ones subject to either homogeneous Dirichlet, homogeneous Neumann or periodic boundary conditions. In the finite line problems considered in this paper, the mass, total momentum and total energy of the NLS equation may not be conserved, i.e., they may not be invariants of the NLS equation in the finite line. Furthermore, the total momentum (cf. Eq. (11)) is also calculated here since it can be used to assess the influence of the discretization on the velocity of the soliton which is equal to the ratio of the total momentum to the total mass for a soliton in the IVP of the NLS equation. Moreover, it is a good numerical practice to calculate the total momentum in order to check the effect of the spatial discretization on the evaluation of both the first-order spatial derivative and the total energy (cf. Eq. (12)). The total momentum and the total energy of the NLS equation are nearly preserved by the Crank-Nicolson scheme (cf. Eq. (16)) for the IVP of the NLS equation. In this paper, the mass, total momentum and total energy are evaluated numerically by means of the Simpson's rule which is fourth-order accurate [32].

In the numerical simulations of finite line problems presented in this paper, the initial condition corresponding to the exact N -soliton solution truncated to a finite interval has been used. However, this initial condition (cf. Eq. (9)) is mathematically incompatible with the boundary conditions (cf. Eq. (14)). In order to avoid mathematical incompatibilities, the following initial condition was used in the simulations presented in this paper

$$U_0(x) = u(x, 0) + ax^2 + bx + c, \quad (23)$$

where the values of a , b and c were determined in such a manner that the initial condition, i.e., $U_0(x)$, satisfied the homogeneous boundary conditions,

and $u(x, 0)$ is given by Eq. (9). It may be easily shown that, for the Dirichlet problem,

$$a = 0, \quad b = \frac{i}{L} \mathcal{I}m[u(-L, 0)], \quad c = -\mathcal{R}e[u(-L, 0)], \quad (24)$$

for the Neumann problem,

$$a = \frac{1}{2L} \mathcal{R}e[u_x(-L, 0)], \quad b = -i \mathcal{I}m[u_x(-L, 0)], \quad c = 0, \quad (25)$$

and, for the Robin problem,

$$\begin{aligned} a &= 0, & b &= \frac{1}{L} (\gamma \mathcal{R}e[u_x(-L, 0)] + i \mathcal{I}m[u(-L, 0)]), \\ c &= \frac{1}{L} \left\{ -(1+i)\gamma^2 \mathcal{R}e[u_x(-L, 0)] + (1-i)\gamma \mathcal{I}m[u(-L, 0)] \right\} - \\ &\quad - \mathcal{R}e[u(-L, 0)] - i\gamma \mathcal{I}m[u_x(-L, 0)], \end{aligned} \quad (26)$$

where $\mathcal{R}e$ denotes real part. It must be noted that the correction to the exact solution of the IVP of the NLS equation used in this paper to avoid mathematical incompatibilities between the initial and boundary conditions in finite line problems is not unique, and that other corrections different from the parabolic one employed here may be used. However, the difference between the parabola chosen here and other possible functions is a minor one because the corrections introduced by the translation of the initial conditions are on the order of $\exp(-AL)$ and, for say, $A=1$ and $L \geq 20$, these differences are very small compared with the soliton's amplitude. Furthermore, simulations have shown that the solutions of the NLS equation with and without translation of the initial conditions nearly yield the same results except for the small numerical errors introduced by the discretization of the NLS equation and boundary conditions.

Symmetric, second-order accurate in space, computational molecules were employed at all the spatial grid points in the periodic problem, while asymmetric, three-point, second-order accurate stencils were introduced at the boundary points for the Dirichlet, Neumann and Robin problems in order to evaluate the total momentum and the total energy.

4 The NLS Equation in the Quarterplane

In this section, the NLS in semi-infinite lines subject to homogeneous Dirichlet or Neumann boundary conditions at $x=0$ is considered in order to analyze the interaction of the soliton with the finite boundary and explain some of the numerical results which will be presented in Section 5 regarding the interaction of solitons with the boundaries in finite line problems.

4.1 The Dirichlet Problem in the Quarterplane

In this section, it is shown that the interaction between a soliton with parameters $\{A_j, V_j, x_{j0}, \phi_{j0}\}$ in the semi-infinite line and a homogeneous Dirichlet boundary condition at $x = 0$ is identical to the interaction between that soliton and another soliton, i.e., its image with respect to the Dirichlet boundary, of parameters $\{A_j, -V_j, -x_{j0}, \pi + \phi_{j0}\}$. It must be noted that the soliton image may also be represented by the parameters $\{-A_j, -V_j, -x_{j0}, \phi_{j0}\}$ which are the ones employed in this paper. For the sake of convenience in what follows, $u_s \equiv \{A, V, x_0, \phi_0\}$ and $\tilde{u}_s \equiv \{-A, -V, -x_0, \phi_0\}$ will be used to define the soliton in the quarterplane and its image with respect to a Dirichlet boundary. In the case of several solitons in the quarterplane, the subscript j

will be used to denote the j -th soliton.

Equations (4) and (5) yield the following result at the boundary, i.e., at $x=0$,

$$\lambda = A + iV/\sqrt{2} = -\tilde{\lambda}, \quad \gamma = \exp(-\lambda x_0/\sqrt{2} + i\lambda^2 t/2 + i\phi_0) = \tilde{\gamma}, \quad (27)$$

while Eq. (3) yields

$$(\gamma^{-1} + \gamma^*) \begin{pmatrix} \frac{1}{\lambda + \lambda^*} & \frac{1}{\lambda - \lambda^*} \\ \frac{1}{-\lambda + \lambda^*} & \frac{1}{-\lambda - \lambda^*} \end{pmatrix} \begin{pmatrix} u_s \\ \tilde{u}_s \end{pmatrix} = \begin{pmatrix} 1 \\ 1 \end{pmatrix}, \quad (28)$$

whose solution is the trivial one, i.e.,

$$u(0, t) = u_s + \tilde{u}_s = 0. \quad (29)$$

Therefore, the superposition of a soliton which is the solution of the IVP of the NLS equation and its image with respect to a Dirichlet boundary is a solution of the NLS equation in the quarterplane with homogeneous Dirichlet boundary conditions at $x=0$.

In order to show that the method of images presented in previous paragraphs for two solitons is also valid for N solitons in the quarterplane with homogeneous Dirichlet boundary conditions at $x=0$, consider the exact N -soliton solution given by Gordon [30] for the IVP of the NLS equation (cf. Eqs. (2)–(5)) and apply the following induction principle. Assume that the superposition of $(N-1)$ -solitons $\{u_{sj}\}$ and their images $\{\tilde{u}_{sj}\}$ is zero at the in a process of soliton-image pair cancellation. In order to show that the addition of another soliton and its image to the $(N-1)$ -solitons and their images is also zero, we first introduce the following notation

$$\eta_{jk} = \gamma_j^{-1} + \gamma_k^*, \quad \mu_{jk}^{-1} = \lambda_j + \lambda_k^*, \quad \nu_{jk}^{-1} = \lambda_j - \lambda_k^*, \quad (30)$$

and note that, for the homogeneous Dirichlet boundary condition at $x=0$,

$$\lambda_j = -\tilde{\lambda}_j, \quad \gamma_j = \tilde{\gamma}_j. \quad (31)$$

From the induction hypothesis,

$$\tilde{u}_{sj} = -u_{sj}, \quad \text{for } j = 1, 2, \dots, N-1, \quad (32)$$

while, from Eq. (3), the following linear system of $2N$ -equations must be satisfied

$$\sum_{k=1}^{N-1} \eta_{jk}(\mu_{jk} - \nu_{jk})u_{sj} + \eta_{jN}(\mu_{jN}u_{sN} + \nu_{jN}\tilde{u}_{sN}) = 1, \quad (33)$$

$$\sum_{k=1}^{N-1} \eta_{jk}(-\nu_{jk} + \mu_{jk})u_{sj} + \eta_{jN}(-\nu_{jN}u_{sN} - \mu_{jN}\tilde{u}_{sN}) = 1, \quad (34)$$

$$\sum_{k=1}^{N-1} \eta_{Nk}(\mu_{Nk} - \nu_{Nk})u_{sN} + \eta_{NN}(\mu_{NN}u_{sN} + \nu_{NN}\tilde{u}_{sN}) = 1, \quad (35)$$

$$\sum_{k=1}^{N-1} \eta_{Nk}(-\nu_{Nk} + \mu_{Nk})u_{sN} + \eta_{NN}(-\nu_{NN}u_{sN} - \mu_{NN}\tilde{u}_{sN}) = 1, \quad (36)$$

for $j = 1, 2, \dots, N-1$.

Substraction of the last two equations yields

$$(\mu_{NN} + \nu_{NN})(u_{sN} + \tilde{u}_{sN}) = 0, \quad (37)$$

which indicates that the introduction of a new soliton is compensated by its image. Therefore, the set of N solitons and of their N images satisfies the homogeneous Dirichlet boundary condition at $x=0$.

In order to illustrate the method of images developed in this section, the interaction of two solitons of $A_1=V_1=-A_2=-V_2=q=1$, $x_{01}=0$, $x_{02}=100$, and $\phi_{01}=\phi_{02}=0$ is illustrated in Figure 1. The results presented in Figure 1

simulate the interaction of a soliton with a homogeneous Dirichlet boundary condition at $x=50$ in a quarterplane problem, and indicate that the amplitude of both solitons increases as they approach $x=50$ and that both solitons rebound from each other with the same amplitude and speed as those prior to their collision or interaction with the finite boundary.

4.2 The Neumann Problem in the Quarterplane

In this section, we show that the interaction of a soliton with a Neumann boundary in a quarterplane problem is identical to the collision between two solitons of the same amplitude and initial phase, but of opposite velocities. For a soliton with parameters $\{A_j, V_j, x_{j0}, \phi_{j0}\}$, its image with respect to a Neumann boundary located at $x = 0$ has the parameters $\{A_j, -V_j, -x_{j0}, \phi_{j0}\}$. Without loss of generality, consider a semi-infinite line problem with the homogeneous Neumann boundary condition at $x = 0$, and a soliton with parameters $u_s \equiv \{A, V, x_0, \phi_0\}$ and its Neumann-image $\tilde{u}_s \equiv \{A, -V, -x_0, \phi_0\}$.

From Eqs. (4) and (5),

$$\lambda = A + iV/\sqrt{2} = \tilde{\lambda}^*, \quad (38)$$

$$\gamma = \exp(\lambda(x - x_0)/\sqrt{2} + i\lambda^2 t/2 + i\phi_0) = e^{\lambda x/\sqrt{2}} \zeta, \quad (39)$$

$$\tilde{\gamma} = \exp(\lambda^*(x + x_0)/\sqrt{2} + i\lambda^{*2} t/2 + i\phi_0) = e^{\lambda^* x/\sqrt{2}} \zeta^{*-1}, \quad (40)$$

and Eq. (3) becomes

$$M(x, t) = \begin{pmatrix} \frac{e^{-\lambda x/\sqrt{2}} \zeta^{-1} + e^{\lambda^* x/\sqrt{2}} \zeta^*}{\lambda + \lambda^*} & \frac{e^{-\lambda x/\sqrt{2}} \zeta^{-1} + e^{\lambda x/\sqrt{2}} \zeta^{-1}}{2\lambda} \\ \frac{e^{-\lambda^* x/\sqrt{2}} \zeta^* + e^{\lambda^* x/\sqrt{2}} \zeta^*}{2\lambda^*} & \frac{e^{-\lambda^* x/\sqrt{2}} \zeta^* + e^{\lambda x/\sqrt{2}} \zeta^{-1}}{\lambda + \lambda^*} \end{pmatrix}, \quad (41)$$

whose value at the finite boundary, i.e., M_0 , is

$$M_0(t) = \begin{pmatrix} \frac{\zeta^{-1} + \zeta^*}{\lambda + \lambda^*} & \frac{\zeta^{-1}}{\lambda} \\ \frac{\zeta^*}{\lambda^*} & \frac{\zeta^* + \zeta^{-1}}{\lambda + \lambda^*} \end{pmatrix} \equiv \begin{pmatrix} \mu & \nu \\ \rho & \mu \end{pmatrix}, \quad (42)$$

while its first-order spatial derivative at the same point is

$$\dot{M}_0(t) = \begin{pmatrix} \frac{-\lambda\zeta^{-1} + \lambda^*\zeta^*}{\sqrt{2}(\lambda + \lambda^*)} & 0 \\ 0 & \frac{-\lambda^*\zeta^* + \lambda\zeta^{-1}}{\sqrt{2}(\lambda + \lambda^*)} \end{pmatrix} \equiv \begin{pmatrix} \epsilon & 0 \\ 0 & -\epsilon \end{pmatrix}, \quad (43)$$

where the dot denotes partial differentiation with respect to x .

In order to prove that the superposition of a soliton and its image has a first-order spatial derivative equal to zero at the \pm , Eq. (3) may be written as

$$M(x, t)u(x, t) = c \equiv \begin{pmatrix} 1 \\ 1 \end{pmatrix}, \quad (44)$$

and differentiated with respect to x to obtain

$$\dot{M}(x, t)u(x, t) + M(x, t)\dot{u}(x, t) = 0. \quad (45)$$

Equation (45) yields

$$\dot{u}(x, t) = -M^{-1}(x, t)\dot{M}(x, t)M^{-1}(x, t)c, \quad (46)$$

while Eq. (44) at the boundary yields

$$u_s = \frac{1}{|M_0|}(\mu - \nu), \quad \tilde{u}_s = \frac{1}{|M_0|}(\mu - \rho), \quad (47)$$

which multiplied by \dot{M}_0 gives

$$\dot{M}_0 \begin{pmatrix} u_s \\ \tilde{u}_s \end{pmatrix} = \frac{\epsilon}{|M_0|} \begin{pmatrix} \mu - \nu \\ -\mu + \rho \end{pmatrix}. \quad (48)$$

Finally, Eq. (46) yields

$$\dot{u}_s = -\frac{\epsilon}{|M_0|^2}(\mu^2 - \nu\rho), \quad (49)$$

$$\dot{\tilde{u}}_s = -\frac{\epsilon}{|M_0|^2}(-\mu^2 + \nu\rho), \quad (50)$$

that clearly add to zero. Therefore, the superposition of a soliton and its image with respect to a Neumann boundary satisfies homogeneous Neumann boundary conditions at that boundary, and is a solution of the NLS in the quarterplane subject to homogeneous Neumann boundary conditions at $x=0$.

Based on the results obtained in previous paragraphs, it may be thought that an induction argument similar to the one employed in Section 4.1 could be used to demonstrate the validity of the method of images for the N -soliton solution of the NLS equation in the quarterplane subject to homogeneous Neumann boundary conditions at $x=0$. However, the tediousness of the algebra involved has not allowed us as yet to present an elegant proof. Following the same type of reasoning as in the proof for only one soliton and its image presented above and using Matlab, we have numerically studied the method of images for a wide range of parameters with up to ten solitons. Based on these studies, we have numerical evidence on the validity of the method of images presented in this section for quarterplane problems subject to homogeneous Neumann boundary conditions at $x=0$.

In order to illustrate the method of images developed in this section, the interaction of two solitons of $A_1=V_1=A_2=-V_2=q=1$, $x_{01}=0$, $x_{02}=100$, and $\phi_{01}=\phi_{02}=0$ is illustrated in Figure 2. The results presented in Figure 2 simulate the interaction of a soliton with a homogeneous Neumann boundary condition at $x=50$ in a quarterplane problem, and indicate that the amplitude

of both solitons increases as they approach $x=50$. The results shown in Figure 2 may be interpreted as either the rebounding of a soliton from a Neumann boundary or the penetration of two colliding solitons. In either case, the solitons re-emerge from their interaction with the same amplitude and speed as those prior to their collision.

5 The NLS Equation in the Finite Line

In this section, some numerical results of the NLS equation in finite lines subject to homogeneous Dirichlet, Neumann and Robin boundary conditions are presented and compared with those corresponding to periodic boundary conditions and IVP problems. Special emphasis is placed on the interaction of the solitons with the boundaries of the finite line. The results presented in this section correspond, unless otherwise stated, to $q=A=V=1$, $\phi_0=x_0=0$, $L=50$, $\Delta t=0.01$ and $\Delta x=0.25$.

5.1 The Dirichlet Problem

Some sample results corresponding to the solution in the NLS equation in the finite line subject to homogeneous Dirichlet boundary conditions at both boundaries, here referred to as the Dirichlet problem, are presented in Figure 3. Note that, since the Dirichlet problem is invariant under reflections in x , only the interaction of the soliton with the right boundary is presented in this section.

Figure 3 (top left) indicates that, as the soliton approaches the right boundary, its maximum amplitude increases due to the fact that the soliton's

amplitude is zero at the boundary, i.e., the soliton cannot penetrate into the boundary. Furthermore, the soliton's velocity decreases as the soliton approaches the right boundary. Note that, during the interaction of the soliton with the boundary, a bump appears in the soliton's tail away from the boundary. The amplitude of the bump's minimum decreases as the soliton approaches the right boundary.

When the soliton's velocity reaches a zero value, the bump's minimum also reaches a zero value, and the soliton's maximum amplitude is largest. Thereafter, the soliton rebounds from the right boundary and its largest amplitude decreases until both its speed and maximum amplitude recover the values that they had prior to the collision of the soliton with the right boundary.

The results presented in Figure 3 (top left) are nearly identical to those of Figure 1 as it should be expected since, for the finite problem considered here, the distance between the left and right boundaries, i.e., $2L=100$, is very large compared with the soliton's width and the interaction of the soliton with the right boundary in such a case is expected to be nearly identical to that of the quarterplane problem presented in Section 4.1.

The results presented in Figure 3 (top right) indicate that the total mass is conserved during the soliton propagation and interaction with the right boundary as in the IVP of the NLS equation. This result is consistent with the integral of Eq. (13) over the spatial domain.

The total momentum illustrated in Figure 3 (bottom left) is constant when the soliton is far away from the boundaries. During the collision between the soliton and the , the total momentum experiences a change in sign

caused by the change in the direction of propagation after the soliton rebounds from the boundary. Figure 3 (bottom left) also shows that the total momentum changes sign smoothly during the collision with the boundary.

The Hamiltonian or total energy is constant during the soliton propagation, but it suffers a great change as the soliton collides with the right boundary as illustrated in Figure 3 (bottom right) which indicates that the total energy of the soliton first decreases as the soliton approaches the boundary and then increases as the soliton recedes from the boundary, until it recovers the constant value that it had prior to the interaction of the soliton with the right boundary. The behaviour of the total momentum and total energy described in previous paragraphs is identical for all the collisions with boundaries subject to homogeneous Dirichlet boundary conditions.

5.2 The Neumann Problem

The interaction of a soliton with a homogeneous Neumann boundary condition is quite different from that observed in the Dirichlet problem as illustrated in Figure 4 (top left). This figure shows that the soliton penetrates into the right boundary due to the zero slope condition imposed there. This penetration process is accompanied by an increase in the soliton's amplitude at the boundary and a decrease in the soliton's maximum amplitude away from the boundary; between these two relative maxima, the soliton's amplitude exhibits a relative minimum.

Some time during the interaction of the soliton with the right boundary, the maximum amplitude at the boundary becomes equal to that away from the boundary which keeps on decreasing with a decreasing velocity. Later

on, the largest amplitude of the soliton occurs at the boundary; therefore, the location of the soliton's maximum amplitude undergoes a jump from the interior of the domain to the boundary, while the soliton's minimum amplitude keeps on decreasing as the soliton approaches the right boundary.

When the soliton's minimum amplitude is exactly zero, the soliton's maximum amplitude at the boundary is largest, and the maximum amplitude away from the boundary is smallest and has a zero velocity. At this moment, the soliton's maximum amplitudes at the boundary and in the domain are twice and one half, respectively, the amplitude of the soliton prior to the collision with the boundary.

As the soliton rebounds from the right boundary, the amplitude at the boundary decreases while the maximum and minimum amplitudes away from the boundary increase, the rebounding process is opposite to the collision one, and the rebounding soliton recovers both the shape and the speed of the colliding one.

It is important to note that, after the rebound from the boundary, the solitons of both the Dirichlet and the Neumann problems move with the same velocity and are identical except for a phase difference of π radians. Furthermore, since the NLS equation subject to homogeneous Neumann boundary conditions represents a symmetric boundary value problem, i.e., the equation and the boundary conditions are invariant under reflections in x , the interaction of the soliton with the right boundary is identical to that with the left one. Therefore, a soliton which undergoes two collisions one with the right boundary followed by another one with the left boundary will recover its original shape, velocity and phase if both boundaries are subject to

homogeneous Dirichlet or Neumann boundary conditions. Moreover, after a collision with the right boundary followed by another one with the left boundary, there is no phase difference between the Dirichlet and Neumann solitons.

The results presented in Figure 4 (top left) are nearly identical to those of Figure 2 as it should be expected since, for the finite line problem considered here, the distance between the left and right boundaries, i.e., $2L=100$, is very large compared with the soliton's width and the interaction of the soliton with the right boundary in such a case is expected to be nearly identical to that of the quarterplane problem presented in Section 4.2.

Figure 4 (top right) indicates that the mass is nearly conserved during the soliton's propagation and interaction with the homogeneous Neumann boundary condition as in the IVP of the NLS equation. According to Eq. (13), the mass should be strictly conserved for the Neumann problem; therefore, the non-constancy of the mass illustrated in Figure 4 (top right) is entirely due to small, numerical errors.

Figure 4 (bottom) also shows that the total momentum is constant when the soliton is far away from the boundaries and changes sign during the soliton's interaction with the right boundary. This change is due to the change in the soliton's velocity after the soliton rebounds from the boundary. Figure 4 (bottom left) also shows that the total momentum first undergoes a small increase in value at the beginning of the collision process, and then rapidly changes its sign reaching a zero value at the same time as that of the Dirichlet problem. The different slopes of Figure 3 (bottom left) and Figure 4 (bottom left) indicate that the sign change in the total momentum

is faster in the Neumann problem than in the Dirichlet one.

Figure 4 (bottom right) illustrates that the total energy first increases slightly at the beginning of the collision process and then decreases until it reaches a minimum value. Thereafter, it increases a little bit until it recovers the constant value that it had prior to the collision with the boundary. Note that the slope and minimum value of the total energy are steeper and smaller, respectively, for the Neumann problem than for the Dirichlet one.

The behaviour of the total momentum and the total energy described in previous paragraphs is identical for all the collisions with boundaries subject to homogeneous Neumann boundary conditions owing to the invariance of the Neumann problem under mirror reflections in x .

5.3 The Robin Problem

Since the NLS equation in the finite line subject to homogeneous Robin boundary conditions at both boundaries is not a symmetric problem, the interaction between a soliton with the right boundary is expected to be different from that with the left one. For this reason, the interactions of the soliton with the right and left boundaries are discussed separately in the next paragraphs.

Figure 5 (top left) shows the first collision of a soliton with the right boundary for $\gamma = 1$ and indicates that, prior to the interaction with the right boundary, the soliton behaves as in the IVP of the NLS equation, i.e., it does not notice the presence of the boundary. At the beginning of the collision with the right boundary, the soliton's amplitude at the boundary has a value approximately equal to half the sum of those of the Dirichlet and Neumann

problems at the same boundary (cf. Sections 5.1 and 5.2). When the soliton is near enough to the boundary, its behaviour changes drastically. First of all, the soliton penetrates into the boundary, but it seems to be retained in a kind of boundary layer that is formed at the right boundary and that seems to trap and delay the soliton's motion with respect to those observed in the Neumann and Dirichlet problems.

Figure 5 (top left) also indicates that the value of the slope of the amplitude at the right boundary is slightly smaller than that of the Dirichlet problem and that the soliton penetrates into the boundary with a slightly larger speed than that of the Neumann problem before it stops. This will be illustrated in greater detail in Section 5.4.

Figure 5 (top left) also shows that the largest amplitude of the soliton does not occur at the boundary (compare with the Neumann problem, cf. Figure 4 (top left)). The soliton does, however, show a minimum and a maximum amplitude near the right boundary. When the minimum amplitude reaches a zero value, the maximum amplitude away from the boundary is largest and the soliton velocity is nil. After the collision, the soliton rebounds from the right boundary undergoing a process similar, but opposite to that prior to the collision, it appears to recover its original shape and speed, and it exhibits a delay in its position with respect to the periodic, Neumann and Dirichlet problems caused by the boundary layer at the right boundary. This delay will be illustrated in greater detail in Section 5.4.

Figure 5 (top right) illustrates the collision that the soliton undergoes with the left boundary after having interacted previously with the right one, and indicates that, at the beginning of the collision, the soliton seems to

behave as in the collision with the right boundary. However, the soliton does not seem to penetrate into the left boundary; rather, a hump is formed ahead of the soliton, and this hump penetrates into the boundary.

The hump has a similar but opposite slope to that of the Dirichlet problem, and joins the soliton's maximum amplitude with a minimum of very large curvature. During the collision, the hump's amplitude increases, the curvature of the minimum amplitude also increases, the soliton's maximum amplitude does not reach as high values as in the collision with the right boundary but is larger than the hump's amplitude, and another minimum of decreasing amplitude appears in the soliton's tail. The appearance of both the hump and the minimum near to the left boundary may be caused by the boundary layer formed there which does not allow the soliton to penetrate into the boundary.

When the minimum amplitude in the soliton's tail reaches a zero value, the maximum amplitude of the soliton, the hump's amplitude and the minimum amplitude near the boundary are largest, whereas the soliton's velocity is nil.

In the rebounding process, the soliton appears to show an opposite behaviour to that prior to the collision; however, the boundary layer at the left boundary traps the soliton's tail in such a manner that, after the collision, the soliton re-emerges with a little hump localized at the left boundary whose amplitude remains nearly constant as the soliton keeps on propagating towards the right boundary.

As indicated in Figures 3–5, the location of the soliton's maximum amplitude in the Robin problem is delayed when it collides with the right boundary

with respect to those corresponding to the Dirichlet and Neumann problems. However, after the collision with the left boundary, no delay with respect to the solitons observed in the Neumann and Dirichlet problems is observed. This will be illustrated in greater detail in Section 5.4.

In order to examine further interactions of the soliton with the boundaries, the amplitudes at the right and left boundaries are presented in Figure 5 (bottom left) and Figure 5 (bottom right), respectively, as functions of time for $\gamma = 1$ and $\gamma = -1$. For $\gamma = 1$, the amplitude at the right boundary is zero except when the soliton collides with that boundary (cf. Figure 5 (bottom left)). The amplitude at the left boundary (cf. Figure 5 (bottom right)) clearly indicates the formation of a hump in the first collision with that boundary. The hump's amplitude increases as the soliton collides with the left boundary until about $t = 900$, it then decreases until about $t = 1800$. Further collisions with the left boundary indicate that the hump's dynamics is periodic with a period of about nine collisions with that boundary. This periodic behaviour is studied in greater detail in Section 5.5.

Figure 5 (bottom right) also indicates that the hump's amplitude does not change as the soliton propagates from one boundary to the other one and when the soliton collides with the right boundary. Furthermore, the results presented in Figure 5 (bottom) are qualitatively and quantitatively different from those observed in the Dirichlet and Neumann problems (cf. Figures 3 and 4) where subsequent collisions with the boundaries preserve the soliton's original shape and velocity, and are due to the lack of invariance of the Robin problem under mirror reflections in x .

When $\gamma = -1$, no hump appears on the left boundary; however, a hump

is formed at the right boundary due to the asymmetry of the homogeneous Robin boundary conditions. This is illustrated in Figure 5 (bottom) which shows that the dynamics and period of the hump at the right boundary for negative values of γ are exactly the same as those observed in the left hump for positive values of γ , except for the numerical errors introduced by the discretization which cause slight variations in the hump's amplitude.

For values of γ different from 1 and -1 , the collision of the soliton with the boundaries is similar to that of the Neumann problem for $|\gamma| \gg 1$ or the Dirichlet one for $|\gamma| \ll 1$, as it should be expected (cf. Eq. (14)). For values of $|\gamma| = O(1)$, the interaction of the soliton with the Robin boundaries is similar to that for $|\gamma| = 1$.

Numerical experiments not included here indicate that the amplitude and frequency of the hump's recurrent phenomena, the penetration of the soliton into the boundaries, the phase shift introduced in the collisions with the boundaries and the delay in the location of the maximum amplitude that the soliton experiences upon colliding with a Robin boundary depend strongly on γ and are largest for $|\gamma| = 1$. These numerical experiments also indicate that the dynamics of the left and right humps are nearly periodic with periods of about 9 and 2 collisions for $\Delta x = 0.25$ and 0.0625 , respectively, and that the humps exhibit some kind of noise or oscillations, the magnitude of which decreases as the time step is decreased. However, the trends shown in Figure 5 are qualitatively independent of the spatial grid size employed in the calculations.

Figures 6–8 show a detailed view of the mass, total momentum and total energy for several values of γ as the soliton collides with the right and left

boundaries. Figure 6 indicates that the mass suffers some changes, but it recovers the value that it had prior to the collision, after the soliton rebounds from the right and left boundaries. For positive values of γ , the collisions with the right and left boundaries produce a peak and a valley in the mass, respectively, whereas, for negative values of γ , the opposite behaviour is observed. The magnitudes of the peak and valley are largest for $|\gamma| \approx 2$ and decrease monotonically as $|\gamma|$ tends to either infinity or zero.

Figure 7 shows that the total momentum maintains a constant value during the soliton propagation and suffers a change in sign when the soliton collides with the right (Figure 7 (left)) and left (Figure 7 (right)) boundaries due to the change in the direction of the soliton velocity after rebound. For $|\gamma| > 2$, the total momentum has a similar behaviour to that observed in the Neumann problem (cf. Figure 4), whereas, for other values of γ , its behaviour is similar to that of the Dirichlet problem (cf. Figure 3). Figure 7 also shows that the largest value of the time derivative of the total momentum increases as $|\gamma|$ is increased, and that topological changes occur near the value $|\gamma| \approx 2$.

Figure 8 indicates that the total energy is constant during the soliton propagation, and that the changes that it undergoes when the soliton collides with the boundaries depend on the value of γ . The total energy recovers the value that it had prior to the collision, after the soliton rebounds from the boundary. For positive values of γ , the total energy exhibits a valley at the right boundary which is deeper than those observed in the Dirichlet and Neumann problems. The smallest magnitude of this valley occurs for a value of γ approximately equal to 2. For more Neumann problems, i.e., for $\gamma \geq 10$, the total energy exhibits a valley with two small peaks surrounding

it when the soliton collides with the right boundary as indicated in Figure 4. These peaks cannot be observed in Figure 8 (left) because of the large scale employed to capture the smallest value of the energy.

In the next collision which occurs at the left boundary, the total energy exhibits a peak, rather than a valley as indicated in Figure 8 (right), except for the more Neumann problems, i.e., $\gamma \geq 10$, not illustrated here for which it shows a valley surrounded by two small peaks, i.e., it exhibits a similar shape to the one observed in the first collision with the right boundary.

The results presented in Sections 5.1 and 5.2 indicate that the Dirichlet and Neumann problems which are limiting cases of the Robin one, have identical dynamics at the left and right boundaries. However, the Robin problem with $|\gamma| \leq 10$ yields some asymmetry caused by the lack of invariance of the Robin boundary conditions under reflections in x .

5.4 The Soliton's Location and Maximum Amplitude

Figure 9 (left) shows the maximum amplitude of the soliton as a function of time for the periodic, Dirichlet and Neumann problems and indicates that, for the periodic problem, the soliton's maximum amplitude is nearly one except for the small oscillations caused by the finiteness of the spatial grid employed in the calculations. For the Dirichlet problem, the soliton's maximum amplitude grows smoothly during the collision of the soliton with the right boundary. Figure 9 (left) also shows that the dynamics of the soliton's maximum amplitude in the Neumann problem is more complex than those of the periodic and Dirichlet ones. In particular, the soliton's maximum amplitude exhibits an initial decrease followed by a rapid and large increase.

However, as indicated in Section 5.2, this complex dynamics is associated with the jump that the location of the maximum amplitude undergoes as the soliton collides with the boundary.

Figure 9 (right) illustrates the location of the soliton's maximum amplitude and the solitons's crossing of the right boundary in the periodic problem although the left boundary is not shown in the figure. Figure 9 (right) also illustrates that the soliton does not penetrate into the boundary in the Dirichlet problem, and that the location of the soliton's maximum amplitude jumps from the interior of the domain to the boundary and vice versa in the Neumann problem. Figure 9 (right) also indicates that the velocity of the soliton is constant when the soliton is sufficiently far away from the boundaries and that no delay between the Dirichlet and Neumann solitons is observed after their collisions with the right boundary.

The soliton's maximum amplitude and its location for the Robin problem are illustrated in Figure 10 as a function of time for several values of γ . Except for the discontinuous change in the location of the maximum amplitude for the more Neumann problems, the results presented in Figure 10 (top) are similar to those presented previously. Figure 10 (bottom) indicates clearly that the delay in the location of the soliton's maximum amplitude after it collides with the boundaries depends on the value of γ , and that the delay produced in a boundary is compensated for by the collision of the soliton with the other boundary.

It must be pointed out that, due to numerical errors, the numerically determined speed of the soliton prior to its collision with the boundaries is slightly smaller than that of the IVP of the NLS equation, i.e., $V=1$. More-

over, these numerical errors and the finite-order approximation used to discretize both the boundary conditions and the NLS equation in the finite line cause a slight difference in the location of the soliton's maximum amplitude in long time integration, e.g., more than ten collisions with each boundary, for the Dirichlet and Neumann problems. Furthermore, the results shown in Figures 3–5 indicate the presence of small-amplitude, background noise or radiation in the tails of the solitons, which is larger for the Neumann problem than for the Dirichlet one. The magnitude of this noise or radiation decreases as the grid is refined, and cannot be clearly appreciated in Figures 3–5 due to the scale of these figures.

5.5 Phase Diagrams, Recurrence and Nonlinear Dynamical Effects

In the results presented in previous sections, a recurrent behaviour has been observed due to the collision of the soliton with the boundaries. In order to analyze this recurrent phenomenon in more detail, the phase diagrams corresponding to the maximum amplitude of the soliton and to the amplitudes at the left and right boundaries are studied in this section. A second-order accurate, finite difference method has been employed to determine the phase diagram velocity.

For the periodic problem, the soliton's propagation is not affected by the boundaries; therefore, its maximum amplitude is constant, and the corresponding phase diagram is a fixed point. Furthermore, the dynamics of the amplitude at the left and right boundaries is the same as that at any point in the finite interval. For this reason, the phase diagram will be only presented

at the point $x=0$.

The amplitude and the time derivative of the amplitude for the exact 1-soliton solution of the IVP of the NLS equation (cf. Eq. (9)) are

$$\psi(t) \equiv |u(0,t)| = A \operatorname{sech}(\mu), \quad \mu = -\frac{A}{\sqrt{2}}(x_0 + Vt), \quad (51)$$

$$\frac{\partial}{\partial t}\psi(t) = -\mu_t \psi(t) \tanh(\mu), \quad (52)$$

which yield the following phase diagram

$$\begin{cases} \dot{\nu} = \frac{A^2 V^2}{2} \left(\psi - \frac{2}{A^2} \psi^3 \right) \\ \dot{\psi} = \nu, \end{cases}$$

whose fixed points are $(\psi, \nu) = (0,0) = (A/\sqrt{2},0) = (-A/\sqrt{2},0)$. A linear stability analysis indicates that the point $(0,0)$ is a saddle point, while the other two are focal points. The third fixed point, however, lacks physical meaning.

Figure 11 (top) shows that the phase diagram corresponding to the exact 1-soliton solution of the IVP or to the periodic problem of the NLS equation resembles that of the unforced Duffing equation [33]. This is not surprising since Ablowitz et al. [29] have indicated that the Duffing equation can be derived from the NLS equation using a method of separation of variables. Therefore, a mass-string system with a cubic nonlinear stiffness may be a good model of the dynamics of the soliton's amplitude for the IVP and periodic problem of the NLS equation.

Figure 11 (top) also shows that the phase diagram of the soliton's amplitude at the right boundary is a fixed point located at the origin of the phase plane for the Dirichlet problem, since the soliton's amplitude is always equal to zero at the boundaries.

The dynamics of the amplitude at the left and right boundaries is identical for the Neumann problem, has been evaluated numerically, and is also illustrated in Figure 11 (top). This figure indicates that the phase diagram for the Neumann problem is similar to that of the periodic boundary conditions; however, its largest amplitude and velocity are about two and twenty, respectively, times larger than those of the periodic problem for $\Delta x = 0.25$, and about twice and the same, respectively, as those of the periodic problem for $\Delta x = 0.0625$ (not shown here). The large velocity differences in the phase diagrams as the grid size is decreased, clearly indicate the coupling between the temporal and spatial phenomena associated with the soliton propagation, while the magnitude of these velocities is mainly due to the steepening of the soliton as it collides with the boundaries.

The phase diagram of the soliton's maximum amplitude for the periodic, Dirichlet and Neumann problems are shown in Figure 11 (bottom). The phase diagram for the periodic problem is the fixed point $(1, 0)$, while that for the Dirichlet one is nearly elliptical except for the oscillations caused by the spatial grid size used in the calculations. Figure 11 (bottom) also indicates that the phase diagram of the soliton's maximum amplitude for the Neumann problem is topologically very different from those of the periodic and Dirichlet ones. In particular, the phase diagram for the Neumann problem clearly indicates the large velocities associated with the jump that the location of the soliton's maximum amplitude undergoes from the interior of the domain to the boundary as the soliton approaches the boundary and from the boundary to the interior of the domain as the soliton rebounds from the boundary (cf. Section 5.2). Figure 11 (bottom) also illustrates the smooth behaviour of

the phase diagram as the soliton propagates from one boundary to the other one, and resembles those observed in relaxation oscillations (cf., e.g., [33]). Figure 11 (bottom) also shows the background noise or radiation introduced by the discretization, which is characterized by a fat point in the phase diagram for the periodic problem.

The closed phase diagrams for the Dirichlet and Neumann problems confirm the recurrent behaviour of solitons in finite lines subject to homogeneous Dirichlet and Neumann boundary conditions at both boundaries.

Figure 12 shows the phase diagrams corresponding to the amplitude at the left and right boundaries for several values of γ . These diagrams are similar to that corresponding to periodic boundary conditions (cf. Figure 11), and indicate that the maximum amplitude at the boundaries increases monotonically from zero to 2 as $|\gamma|$ is varied from zero to infinity and, is almost linear for $\gamma \ll 1$. The maximum velocity of the amplitude at the boundary points is about one half the maximum amplitude there for all values of γ .

As shown in Section 5.3, the lack of invariance of the Robin problem under mirror reflections in x results in the formation of a boundary layer near to the left boundary for $\gamma = O(1)$. This boundary layer traps the soliton and creates a hump at the left boundary. For negative values of $|\gamma| = O(1)$, a hump is formed at the right boundary, and this hump exhibits exactly the same dynamics as that of the left one as indicated in Figure 5. For this reason, only the dynamics of the hump formed at the left boundary will be discussed in the following paragraphs.

The phase diagrams corresponding to the amplitudes at the left and right boundaries are presented in Figure 13 (left) and Figure 13 (right), respec-

tively. Figure 13 (right) indicates that the phase diagram of the amplitude at the right boundary coincides with that of the periodic problem, whereas that of the amplitude at the left boundary closes upon itself after nine collision of the soliton with that boundary, for $\gamma = 1$. For $\gamma = -1$, no hump is formed at the left boundary and the phase diagram of the amplitude at that boundary coincides with that of the periodic problem, whereas the phase diagram of the amplitude at the right boundary closes upon itself after nine collisions of the soliton with that boundary. As shown in Section 5.3, the nonlinear dynamics of the hump is very sensitive to the spatial grid size and to the value of γ ; small changes in γ or in the spatial grid size result in large changes in both the period and the maximum amplitude of the hump's oscillations.

The phase diagrams of the boundary amplitude shown above indicate that the Duffing equation may be used to study the dynamics of solitons in finite lines with homogeneous Robin boundary conditions if some forcing is introduced in that equation to represent, in some manner, the boundary layers that appear at the boundaries of finite lines.

The phase diagram corresponding to the soliton's maximum amplitude in a finite line with homogeneous Robin boundary conditions is presented in Figures 14 and 15 for several values of γ . For $\gamma = 1.0$, the phase diagram presents two lobes (cf. Figure 14). The lobe of larger amplitude, here referred to as the first lobe, is caused by the collision of the soliton with the right boundary where no hump is formed, and the amplitude of this lobe is larger than the maximum amplitude of the Dirichlet problem. The other, smaller lobe, here referred to as the second lobe, is caused by the collision of the soliton with the left boundary where a hump which traps and delays the

soliton is formed. The maximum amplitude of the second lobe is smaller than the maximum amplitude of the Dirichlet problem. The amplitude of the second lobe decreases whereas that of the first one increases as γ is increased from one.

For a value of $\gamma \approx 1.1$, the results presented in Figure 15 indicate that the second lobe has a different shape than the elliptical one described in Figure 14 and exhibits an additional lobe, here referred to as third lobe, which is characterized by very high velocities due to the fact that the hump's amplitude becomes equal to or exceeds the largest amplitude of the soliton away from the boundary (cf. Section 5.2). When this occurs the velocity shown in the phase diagram increases rapidly as indicated in the Neumann problem. The amplitudes of the first and second lobes increase and decrease, respectively, while that of the third lobe increases quite rapidly, as γ is increased. For $\gamma \approx 2$, the second lobe has nearly disappeared, while the third lobe is as large as the first one.

For $\gamma > 2$, the third lobe has approximately the shape of half an ellipse connected with a very steep, nearly straight line to a nearly triangular shape (cf. Figure 14). For still larger values of γ , the amplitude of the third lobe is larger than that of the first one, which, in turn, acquires a similar shape to that of the third lobe (cf. Figure 14). For $\gamma = \infty$, i.e., for Neumann boundary conditions, the first and third lobes are identical, indicating that these lobes collapse into only one as γ tends to infinity. Since the NLS equation subject to Neumann boundary conditions is a symmetric problem in x , the qualitative changes observed in the phase diagrams presented in Figures 14 and 15 are related to the loss of symmetry of that equation in the

finite line as γ is varied.

5.6 Area of the Phase Diagrams

An indication of the topological changes that occur in the phase diagrams as γ is varied can be obtained by evaluating the areas enclosed by them. This evaluation also gives information on the conservation properties of the numerical scheme employed in the calculations. In this section, the areas of the phase diagrams presented in the previous section are calculated.

In order to evaluate the areas of the phase diagrams, it is necessary to account for the numerically-induced noise or background radiation which, in spite of its small amplitude, is responsible for the fat points observed in the phase diagrams, e.g., Figure 11 (bottom), 14 and 15. If the background radiation were used in the evaluation of these areas, noisy results would be obtained. It is, however, possible to reduce this noise by filtering the soliton's maximum amplitude and the amplitude at the boundary points in such a manner that the filtered phase diagram preserves the most important features, i.e., those associated with the collisions of the soliton with the boundaries, of the unfiltered diagrams. The filter used in this paper employs an amplitude threshold to locate the relative minima closest to both the threshold amplitude and the amplitude at the boundary or the soliton's maximum amplitude. Once these minima have been found, only the part of the maximum amplitude and those at the boundaries between these minima are used to draw the filtered phase diagrams whose areas are evaluated numerically by means of Simpson's quadrature rule.

The areas of the phase diagrams corresponding to the amplitude at the

left and right boundaries are illustrated in Figure 16 (top) as functions of the number of collisions of the soliton with the boundaries for several values of γ . This figure indicates that, for $\gamma \gg 0$, the areas of the phase diagrams decrease less than the 0.5% after ten collisions with each boundary, indicating that dissipative effects are small. Figure 16 (top) also indicates that the areas of the phase diagrams decrease in an oscillatory manner and that the largest amplitude of these oscillations is observed for $\gamma = \mathcal{O}(1)$. These oscillations seem to be introduced by both the background radiation and the filter used to evaluate the areas, and are substantially reduced as the spatial grid size is reduced. Note that the background radiation decreases as Δx is decreased.

For $\gamma \ll 1$, the areas of the phase diagrams increase slightly with the number of collisions of the soliton with the boundaries because the magnitude of the background radiation is comparable to or larger than the amplitude at the boundaries. Note that $\gamma = 0$ corresponds to the Dirichlet problem for which the boundary amplitude is exactly zero.

Figure 16 (top) also shows that the areas of the phase diagrams for the boundary points increase monotonically from zero for the Dirichlet problem to about 2.5 for the Neumann one.

The area of the phase diagram corresponding to the soliton's maximum amplitude is also presented in Figure 16 (bottom), which indicates the effects of the background radiation for small values of γ . For very large values of γ , the area of the phase diagrams varies in an irregular manner because of the errors introduced by the filtering technique and, most importantly, by the fact that the location of the soliton's maximum amplitude jumps discontinuously from the interior of the domain to the boundary, and vice

versa. For $\gamma = \mathcal{O}(1)$, the area of the phase diagrams clearly shows the lack of invariance of the Robin problem under mirror reflections in x . For $\gamma \approx 1$, the area of the phase diagram is larger when the soliton collides with the right boundary than when it collides with the left one in agreement with the lobes presented in Figures 14 and 15, and it exhibits some oscillations, the amplitude of which is largest for $\gamma \approx 1.7$ but does not exceed 0.4%.

Figure 17 shows the area of the phase diagrams corresponding to the amplitude at the left and right boundaries (top) and to the soliton's maximum amplitude (bottom) as functions of γ . Note that Figure 17 (top left) and Figure 17 (top right) correspond to the sixth collision of the soliton with the left and right, respectively, boundaries.

The results presented in Figure 17 (top) indicate that the area of the phase diagram corresponding to the amplitude at the left boundary is nearly identical to that corresponding to the amplitude at the right one despite the lack of invariance of the Robin problem under mirror reflections in x . The results presented in Figure 17 (top) must be interchanged for negative values of γ .

Figure 17 (bottom) shows the areas of the phase diagram corresponding to the maximum amplitude for collisions of the soliton with the left and right boundaries as a function of γ . Figure 17 (bottom right) indicates that the area of the phase diagram for collisions of the soliton with the right boundary is larger than that for collisions with the left one, in agreement with the results presented in Figure 16. The largest differences between the areas of the phase diagrams corresponding to collisions of the soliton with the left and right boundaries (cf. Figure 17 (bottom)) are observed for values

of γ between 0.6 and around 1.7, and are due to the formation of a boundary layer near the left boundary which does not allow the soliton to penetrate into that boundary (cf. Section 5.3) and the consequent formation of the first and second lobes shown in Figures 14 and 15.

6 Conclusions

The NLS equation subject to homogeneous Dirichlet, Neumann and Robin boundary conditions in the finite line has been studied numerically by means of a second-order accurate Crank-Nicolson method, employing as initial condition the exact N -soliton solution truncated to the finite line and translated in such a manner so as to avoid mathematical incompatibilities with the boundary conditions.

A method of images similar to the one used in potential theory has also been developed to study the NLS equation in the quarterplane subject to homogeneous Dirichlet or Neumann boundary conditions at the finite boundary. It has been shown that the interaction of a soliton in quarterplane problems with homogeneous Dirichlet boundary conditions is equivalent to the interaction of two solitons of equal and opposite amplitude and velocity and identical phase placed symmetrically with respect to the finite boundary, whereas the interaction of a soliton in quarterplane problems with homogeneous Neumann boundary conditions is equivalent to the interaction of two solitons of equal and opposite velocity and identical phase and amplitude placed symmetrically with respect to the finite boundary.

Numerical simulations of the soliton's interaction with the Dirichlet and

Neumann boundary conditions in finite line problems indicate that the soliton rebounds from the boundaries recovering its shape except for a phase shift and a numerically induced background radiation whose magnitude decreases as the mesh size is decreased. The soliton's amplitude increases and a bump is formed in the soliton's tail during the collision with the Dirichlet boundary. The rebounding process starts when the bump's minimum reaches a zero amplitude, the soliton's amplitude reaches its largest value and the soliton's velocity is exactly zero.

The collision of a soliton with a Neumann boundary in finite lines is qualitatively quite different from that with a Dirichlet one since the amplitude at the boundary increases from zero until a maximum, larger than the soliton's amplitude in the interior of the domain, is reached. Later on, the amplitude at the boundary decreases while the maximum amplitude in the interior increases. As a consequence, the location of the soliton's maximum amplitude behaves discontinuously since it jumps from the interior to the boundary as the soliton approaches it and from the boundary to the interior as the soliton rebounds from the boundary. It has also been shown that the collision process with the left and right boundaries are identical owing to the symmetry of initial-boundary value problems of the NLS equation subject to homogeneous Dirichlet or Neumann boundary conditions in finite lines.

The homogeneous Robin initial-boundary value problem of the NLS equation in the finite line is not invariant under mirror reflections in the spatial coordinate. As a consequence, the collisions between the soliton and the left and right boundaries have different qualitative behaviour. For positive values of the coefficient that defines the Robin boundary conditions, the soliton

penetrates into the right Ω reaching a large amplitude there, and a bump is formed in its tail. This bump behaves as those of the Dirichlet and Neumann problems, but its motion is delayed by some kind of boundary layer that traps the soliton. After the collision with the right boundary, the rebounding soliton is further delayed with respect to those of the Dirichlet and Neumann problems. In the collision with the left Ω , a boundary layer which does not allow for the penetration of the soliton into the Ω and a hump are formed. After the soliton rebounds from the left boundary, the hump's amplitude is almost constant and subsequent collisions with the right Ω are not affected by this hump. However, subsequent collisions with the left Ω increase the hump's amplitude until it reaches a maximum, beyond which, further collisions with this boundary cause a decrease in the hump's amplitude. The magnitude of the period and maximum amplitude of the periodic hump's behaviour depend on the mesh size and are almost independent of the time step used in the numerical calculations. For negative values of γ , a hump is formed near to the right boundary.

For the homogeneous Neumann and Dirichlet boundary conditions, the mass of the soliton is exactly conserved in the finite line, while the total momentum changes sign during the collision process but it recovers the value that it had prior to the collision with the boundary. The total energy decreases and increases as the soliton approaches and recedes from, respectively, the boundary, indicating a transfer of energy between the soliton and the Ω .

For the homogeneous Robin boundary conditions, the mass of the soliton is conserved between collisions, but it increases and decreases as the soliton collides with the right and left boundaries, respectively. The total momentum

changes sign during the collision of the soliton with the boundary, and its largest value takes place for $|\gamma| \approx 2$. The total energy exhibits a valley and a peak for collisions with the right and the left boundaries, respectively, except for $|\gamma| \gg 10$ for which it exhibits only a valley in both boundaries.

The phase diagrams of the soliton amplitude at the boundary points and for the soliton's maximum amplitude indicate the recurrent behaviour of the collisions of the solitons with the boundaries. The phase diagram has been calculated analytically for periodic boundary conditions and exhibits similar trends to those of the cubic Duffing equation. The phase diagram of the maximum amplitude for the Dirichlet boundary conditions has an almost elliptical shape and exhibits some oscillations. For Neumann boundary conditions, the phase diagrams of the amplitude at the _points have the same shape as in the periodic case, while that of the maximum amplitude is topologically very different from those of the Dirichlet case and shows large velocities associated with the jump that the location of the soliton's maximum amplitude experiences upon the collision of the soliton with the boundaries.

For Robin boundary conditions, the phase diagrams for the amplitude at the boundaries are similar to those of the periodic case, but the maximum amplitude reached at the _depends monotonically on $|\gamma|$ and it is 0 for the Dirichlet case and 2 for the Neumann one. For $|\gamma| = \mathcal{O}(1)$, the hump that appears at one of the boundaries causes that the phase diagram closes upon itself after various collisions with this _ . The phase diagram corresponding to the maximum amplitude depends strongly on the value of γ .

The areas of the phase diagrams for both the soliton's maximum amplitude and the amplitudes at the boundaries have been evaluated numerically

by means of a filter in order to eliminate some of the background radiation. The area of the phase diagram of the amplitude at the boundaries decreases slightly in an oscillatory manner due to the dissipative effects introduced by the numerical method, whereas the area of the phase diagram for the soliton's maximum amplitude clearly shows the non-invariance of the homogeneous Robin boundary conditions under mirror reflections in the spatial coordinate which results in larger areas for the collisions of the soliton with the right _than for those with the left one.

Acknowledgments

This research was supported by the Spanish D.G.I.C.Y.T. under Project no. PB91-0767. The second author (F.R.V.) has a fellowship from the Programa Sectorial de Formación de Profesorado Universitario y Personal Investigador, Subprograma de Formación de Investigadores "Promoción General del Conocimiento", from the Ministerio de Educación y Ciencia of Spain.

References

- [1] A. C. Scott, F. Y. F. Chu and W. McLaughlin, The Soliton—A New Concept in Applied Science, *Proc. IEEE* **61**(10) 1443–1483 (1973).
- [2] M. J. Ablowitz and H. Segur, *Solitons and the Inverse Scattering Transform*, SIAM, Philadelphia (1981).
- [3] C. Rogers and W. F. Shadwick, *Bäcklund Transformations and Their Applications*, Academic Press, New York (1982).

- [4] F. Calogero, Why Are Certain Nonlinear PDEs Both Widely Applicable and Integrable?, In *What Is Integrability?*, (Edited by V. E. Zakharov), pp. 1–61, Springer-Verlag, Berlin, (1991).
- [5] V. E. Zakharov and A. B. Shabat, Exact Theory of Two-Dimensional Self-Focusing and One-Dimensional Self-Modulation of Waves in Nonlinear Media, *Sov. Phys. JETP* **34**(1) 62–69 (1972).
- [6] J. A. C. Weideman and B. M. Herbst, Split-Step Methods for the Solution of the Nonlinear Schrödinger Equation, *SIAM J. Numer. Anal.* **23**(3) 485–507 (1986).
- [7] J. M. Sanz-Serna, Methods for the Numerical Solution of the Nonlinear Schrödinger Equation, *Math. Comp.* **43**, 21–27 (1984).
- [8] T. R. Taha and M. J. Ablowitz, Classical and Numerical Aspects of Certain Nonlinear Evolution Equations. II. Numerical, Nonlinear Schrödinger Equation, *J. Comput. Phys.* **55**, 203–230 (1984).
- [9] G. D. Akrivis, Finite Difference Discretization of the Cubic Schrödinger Equation, *IMA J. Num. Anal.* **13**, 115–124 (1993).
- [10] D. F. Griffiths, A. R. Mitchell and J. Ll. Morris, A Numerical Study of the Nonlinear Schrödinger Equation, *Computer Meths. App. Mech. Engrg.* **45**, 177–215 (1984).
- [11] J. Argyris and M. Haase, An Engineer’s Guide to Soliton Phenomena: Application of the Finite Element Method, *Computer Meths. App. Mech. Engrg.* **61**, 71–122 (1987).

- [12] A. B. Shamardan, The Numerical Treatment of the Nonlinear Schrödinger Equation, *Computers Math. Applic.* **19**(4) 67–73 (1990).
- [13] D. J. Kaup, Approximations for the Inverse Scattering Transform, In *Dynamical Problems in Soliton Systems*, (Edited by S. Takeno), pp. 12–22, Springer-Verlag, Berlin, (1985).
- [14] M. J. Ablowitz and P. A. Clarkson, *Solitons, Nonlinear Evolution Equations and Inverse Scattering*, Cambridge University Press, Cambridge (1991).
- [15] C. K. Chu and R. L. Chou, Solitons Induced by Boundary Conditions, In *Advances in Applied Mechanics, Vol. 27*, (Edited by J. W. Hutchinson and T. Y. Wu), pp. 283–302, Academic Press, Boston, (1990).
- [16] C. K. Chu, L. W. Xiang and Y. Baransky, Solitary Waves Induced by Boundary Motion, *Comm. Pure Appl. Math.* **36**, 495–504 (1983).
- [17] R. L. Chou and C. K. Chu, Solitons Induced by Boundary Conditions from the Boussinesq Equation, *Phys. Fluids A* **2**(9) 1574–1584 (1990).
- [18] D. J. Kaup and P. J. Hansen, The Forced Nonlinear Schrödinger Equation, *Physica D* **18**, 77–84 (1986).
- [19] M. J. Ablowitz and H. Segur, The Inverse Scattering Transform: the Semi-Infinite Interval, *J. Math. Phys.* **16**(5) 1054–1056 (1975).
- [20] A. S. Fokas, An Initial-Boundary Value Problem for the Nonlinear Schrödinger Equation, *Physica D* **35**, 167–185 (1989).

- [21] R. F. Bikbaev and V. O. Tarasov, Initial Boundary Value Problem for the Nonlinear Schrödinger Equation, *J. Phys. A: Math. Gen.* **24**, 2507–2516 (1991).
- [22] A. S. Fokas and M. J. Ablowitz, Forced Nonlinear Evolution Equations and the Inverse Scattering Transform, *Stud. Appl. Math.* **80**, 253–272 (1989).
- [23] Y.-C. Ma and M. J. Ablowitz, The Periodic Cubic Schrödinger Equation, *Stud. Appl. Math.* **65**, 113–158 (1981).
- [24] A. R. Osborne, The Hyperelliptic Inverse Scattering Transform for the Periodic, Defocusing Nonlinear Schrödinger Equation, *J. Comput. Phys.* **109**, 93–107 (1993).
- [25] J. P. Boyd, New Directions in Solitons and Nonlinear Periodic Waves: Polycnoidal Waves, Imbricated Solitons, Weakly Nonlocal Solitary Waves, and Numerical Boundary Value Algorithms, In *Advances in Applied Mechanics, Vol. 27*, (Edited by J. W. Hutchinson and T. Y. Wu), pp. 1–82, Academic Press, Boston, (1990).
- [26] P. L. Christiansen, Solitons and Chaos in the Sine-Gordon System, In *Dynamical Problems in Soliton Systems*, (Edited by S. Takeno), pp. 258–261, Springer-Verlag, Berlin, (1985).
- [27] L. Sirovich, J. D. Rodriguez and B. Knight, Two Boundary Value Problems for the Ginzburg-Landau Equation, *Physica D* **43**, 63–76 (1990).
- [28] R. M. Mirie and C. H. Su, Collisions Between Two Solitary Waves. Part 2. A Numerical Study, *J. Fluid Mech.* **115**, 475–492 (1982).

- [29] M. J. Ablowitz and B. M. Herbst and J. A. C. Weideman, Dynamics of Semi-Discretizations of the Defocusing Nonlinear Schrödinger Equation, *IMA J. Numer. Anal.* **11**, 539–552 (1991).
- [30] J. P. Gordon, Interaction Forces Among Solitons in Optical Fibers, *Optics Lett.* **8**(11) 596–598 (1983).
- [31] G. Ben-Yu, The Convergence of a Numerical Method for the Nonlinear Schrödinger Equation, *J. Comput. Math.* **4**(2) 121–130 (1984).
- [32] A. Ralston and Ph. Rabinowitz, *A First Course in Numerical Analysis*, 2nd ed., McGraw-Hill Book Co., New York (1978).
- [33] J. M. T. Thompson and H. B. Stewart, *Nonlinear Dynamics and Chaos*, John Wiley and Sons, Chichester (1986).

Figure Captions

1. Amplitude, $|u|$, of two interacting solitons of $A_1 = V_1 = -A_2 = -V_2 = q = 1$, $x_{01}=0$, $x_{02}=100$, and $\phi_{01}=\phi_{02}=0$ as a function of space and time calculated using the exact N -soliton solution of the NLS equation. Note that $u(50, t) = 0$.
2. Amplitude, $|u|$, of two interacting solitons of $A_1 = V_1 = A_2 = -V_2 = q = 1$, $x_{01}=0$, $x_{02}=100$, and $\phi_{01}=\phi_{02}=0$ calculated using the exact N -soliton solution of the NLS equation. Note that $u_x(50, t) = 0$.
3. Amplitude, $|u|$, (top left), mass (top right), momentum (bottom left) and energy (bottom right) of a soliton colliding with a homogeneous Dirichlet boundary condition located at $x=50$.
4. Amplitude, $|u|$, (top left), mass (top right), momentum (bottom left) and energy (bottom right) of a soliton colliding with a homogeneous Neumann boundary condition located at $x=50$.
5. Amplitude, $|u|$, of a soliton colliding with the right (top left) and the left (top right) boundaries of a finite line subject to homogeneous Robin boundary conditions for $\gamma=1$, and amplitude at the right (bottom left) and left (bottom right) boundaries for $\gamma=1$ (continuous line) and -1 (dashed line).
6. Mass of a soliton colliding with the right (left) and left (right) boundaries of a finite line subject to homogeneous Robin boundary conditions for $\gamma=10$ (continuous line), 2 (dashed line), 1 (dotted-dashed line) and 0.1 (dotted line).

7. Momentum of a soliton colliding with the right (left) and left (right) boundaries of a finite line subject to homogeneous Robin boundary conditions for $\gamma=10$ (continuous line), 2 (dashed line), 1 (dotted-dashed line) and 0.1 (dotted line).
8. Energy of a soliton colliding with the right (left) and left (right) boundaries of a finite line subject to homogeneous Robin boundary conditions. ($\gamma=10$ (continuous line), 2 (dashed line), 1 (dotted-dashed line), 0.1 (dotted line)).
9. Maximum amplitude (left) and location of the maximum amplitude (right) of a soliton colliding with the right boundary of a finite line subject to periodic (continuous line), Dirichlet (dashed line) and Neumann (dotted-dashed line) boundary conditions.
10. Maximum amplitude (top) and location of the maximum amplitude (bottom) of a soliton colliding with the right (left) and left (right) boundaries of a finite line subject to Robin boundary conditions. ($\gamma = 10$ (continuous line), 2 (dashed line), 1 (dotted-dashed line), 0.1 (dotted line)).
11. Phase diagrams of the amplitude at right boundary (top) and of the soliton's maximum amplitude (bottom) for the Neumann (continuous line), Dirichlet (dashed line) and periodic (dotted-dashed line) problems. Note that only one collision with the right boundary is presented, $L=25$ and $\Delta x=0.0625$.

12. Phase diagrams of the amplitude at the left (left) and right (right) boundaries for the collision of a soliton with homogeneous Robin boundary conditions. Note that only one collision with each boundary is presented. ($L=25$, $\Delta x=0.0625$, and $\gamma = 0.1$ (continuous line), 1 (dashed line) and 10 (dotted-dashed line)).
13. Phase diagrams of the amplitude at the left (left) and right (right) boundaries of a finite line subject to homogeneous Robin boundary conditions. Note that five collisions with each boundary are presented. ($\gamma = 1$ (continuous line) and -1 (dashed line)).
14. Phase diagram of the maximum amplitude for a Robin problem. Note that two collisions, one with each boundary, are presented, $L=25$ and $\Delta x=0.0625$. ($\gamma = 0.1$ (continuous line), 1 (dashed line) and 10 (dotted-dashed line)).
15. Phase diagram of the maximum amplitude for a Robin problem. Note that two collisions, one with each boundary, are presented, $L=25$ and $\Delta x=0.0625$. ($\gamma = 1.125$ (continuous line), 1.25 (dashed line) and 1.7 (dotted-dashed line)).
16. Areas of the phase diagrams corresponding to the amplitude at the left (top left) and right (top right) boundaries and to the soliton's maximum amplitude (bottom) as a function of the number of collisions for the Robin problem. Odd (even) collisions correspond to collisions of the soliton with the right (left) boundary. (The symbols *, o, +, and x correspond to $\gamma = 10$, 1.7, 1, and 0.6, respectively).

17. Areas of the phase diagrams corresponding to the amplitude at the left (top left) and right (top right) boundaries and to the maximum amplitude of the soliton for the sixth collision with the left (bottom left) and right (bottom right) boundaries as functions of γ . The values of $\gamma = 0.1, 0.2, 0.4, 0.6, 0.8, 0.9, 1.0, 1.05, 1.075, 1.1, 1.125, 1.25, 1.7, 1.8, 1.9, 2.0, 2.5, 5.0$ and 10 are represented by the natural numbers (gamma codes) from 1 to 19.

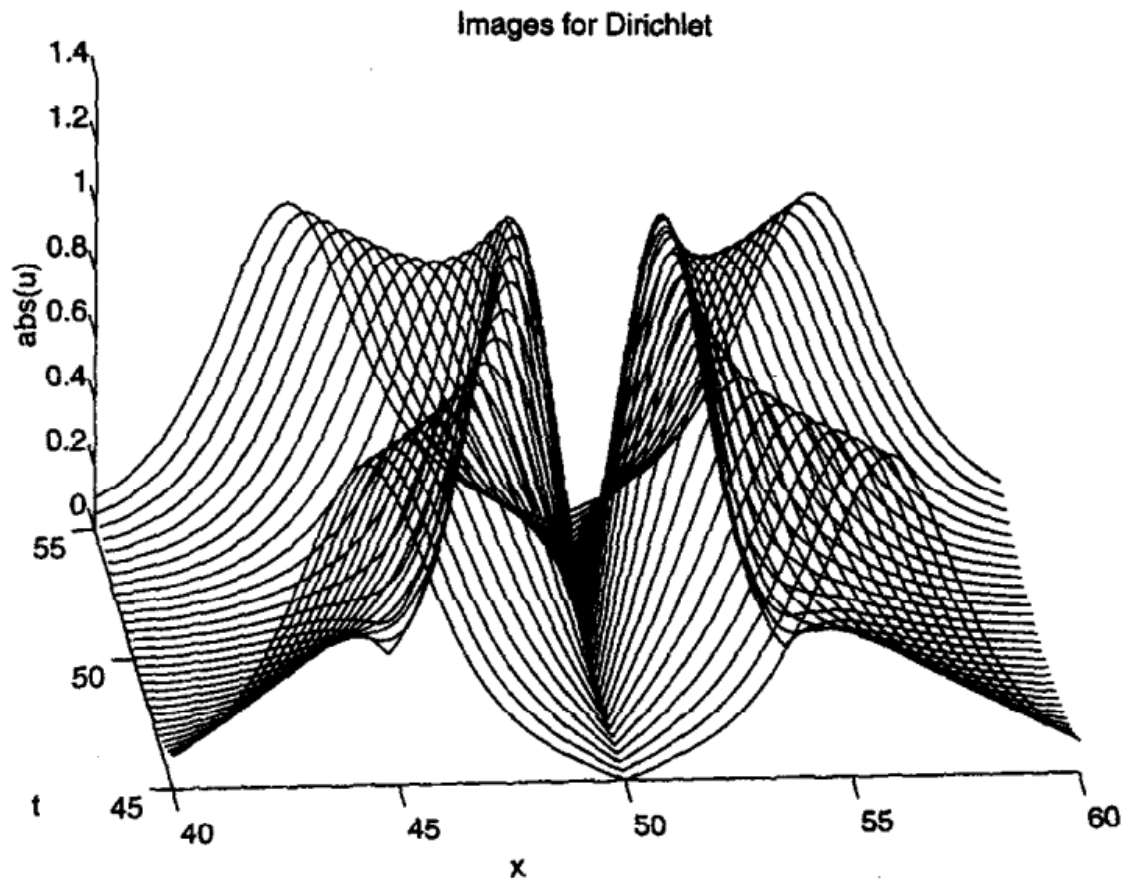


Figure 1. Amplitude, $|u|$, of two interacting solitons of $A_1 = V_1 = -A_2 = -V_2 = q = 1$, $x_{01} = 0$, $x_{02} = 100$, and $\phi_{01} = \phi_{02} = 0$ as a function of space and time calculated using the exact N -soliton solution of the NLS equation. Note that $u(50, t) = 0$.

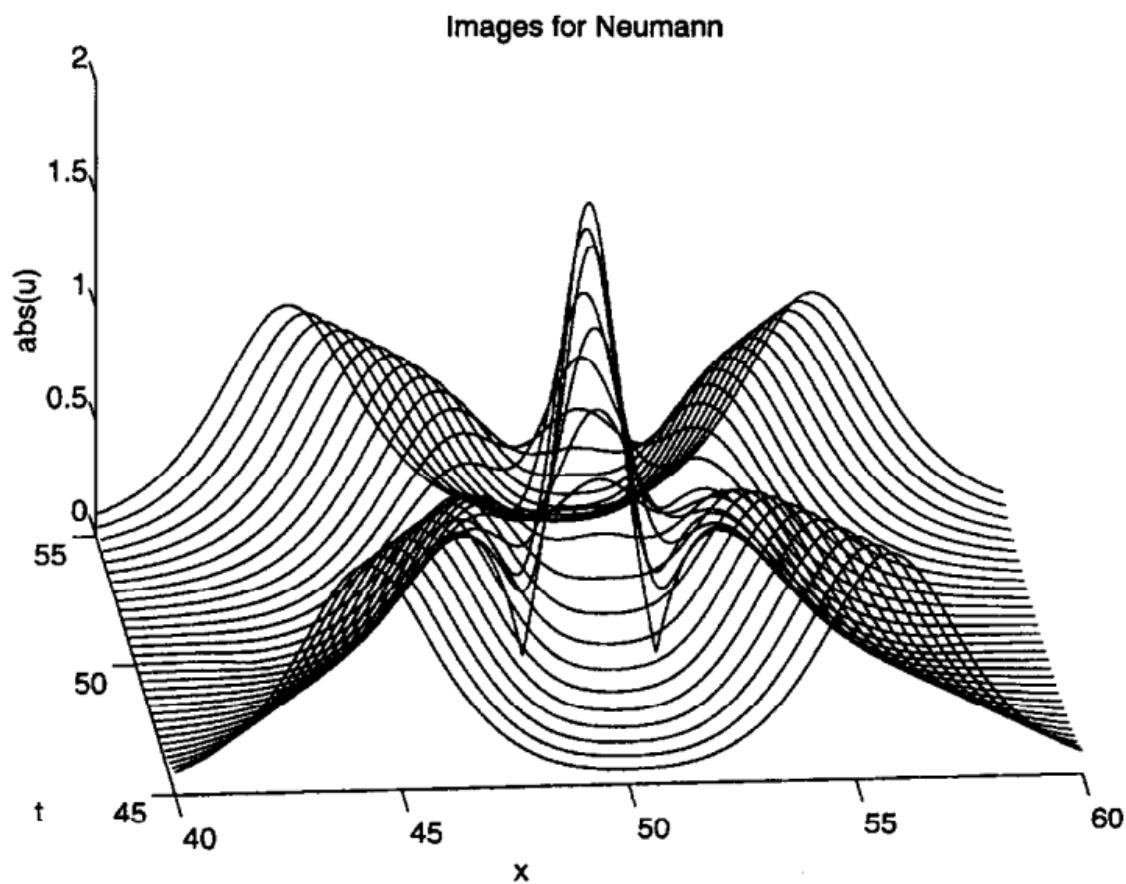


Figure 2. Amplitude, $|u|$, of two interacting solitons of $A_1 = V_1 = A_2 = -V_2 = q = 1, x_{01} = 0, x_{02} = 100$, and $\phi_{01} = \phi_{02} = 0$ calculated using the exact N -soliton solution of the NLS equation. Note that $u_x(50, t) = 0$.

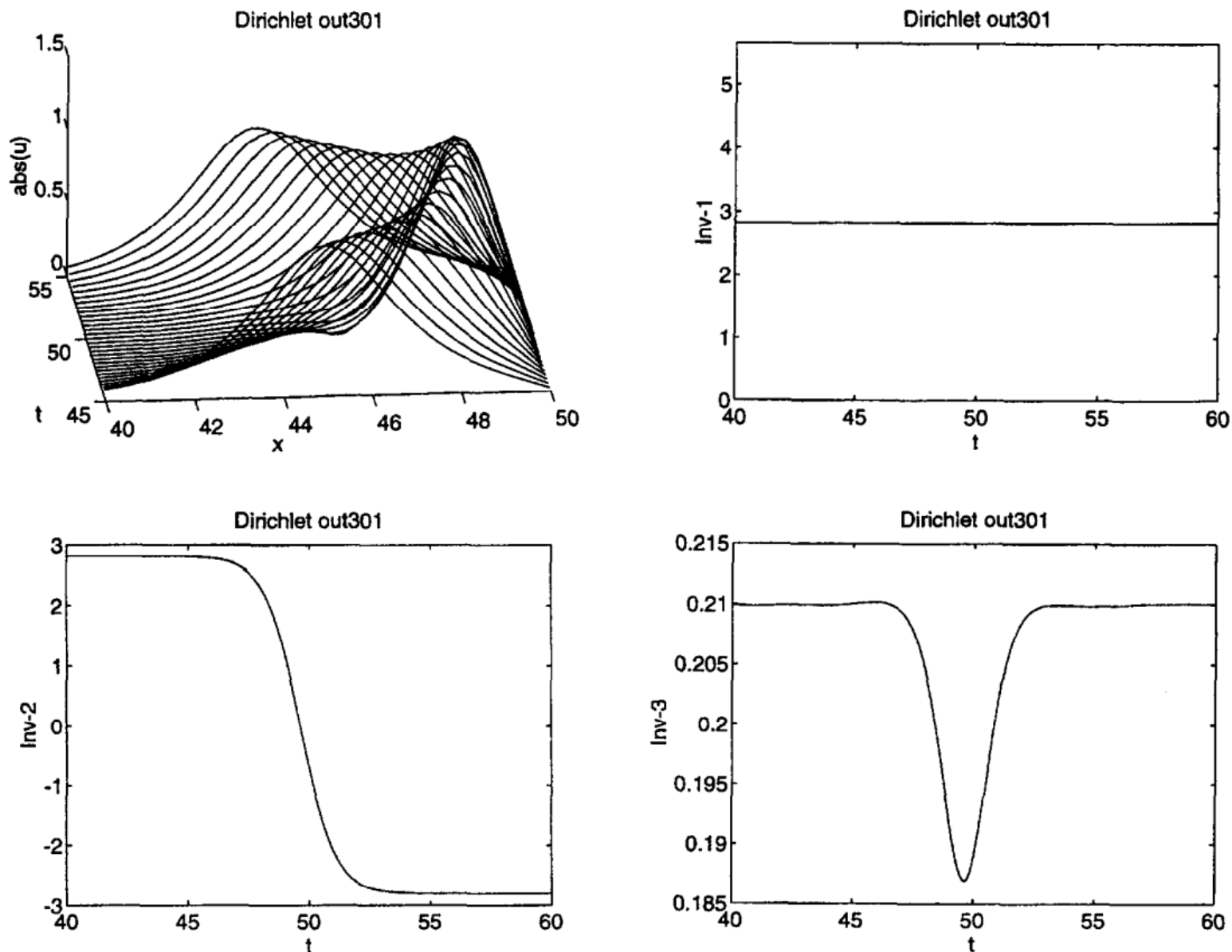


Figure 3. Amplitude, $|u|$, (top left), mass (top right), momentum (bottom left) and energy (bottom right) of a soliton colliding with a homogeneous Dirichlet boundary condition located at $x = 50$.

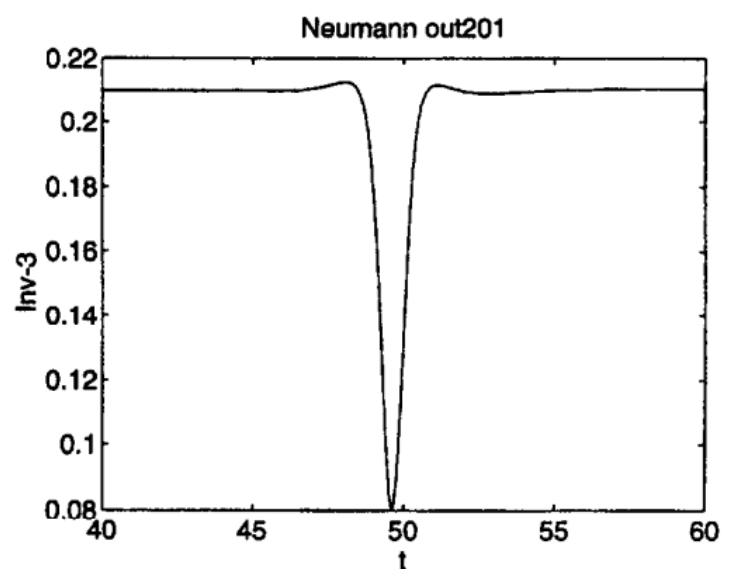
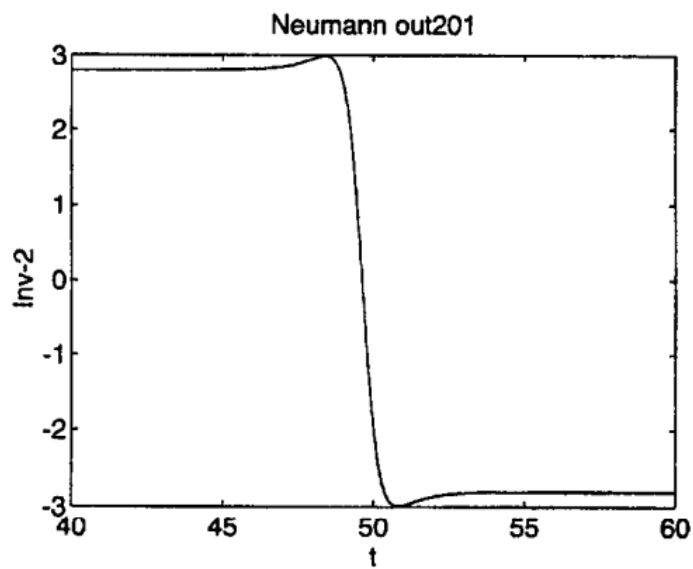
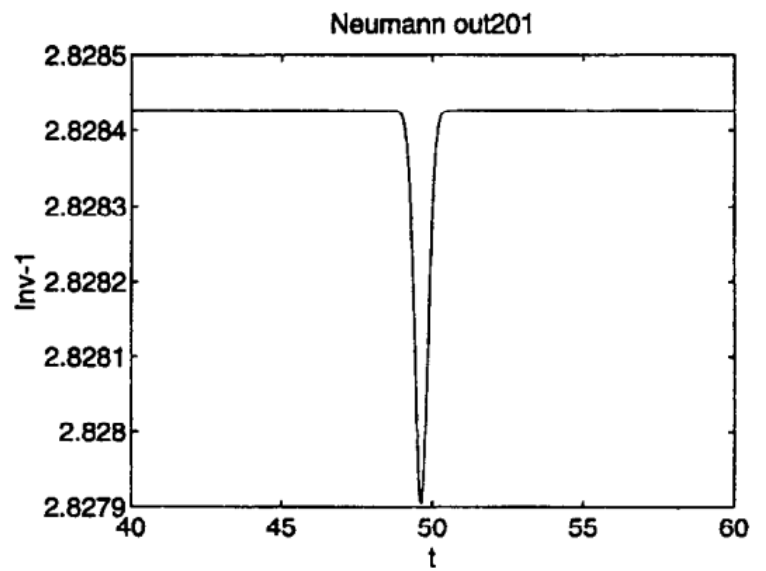
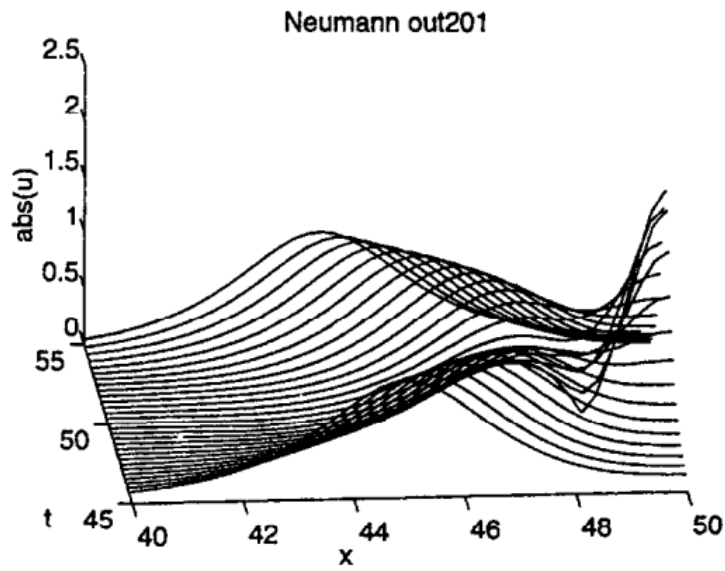
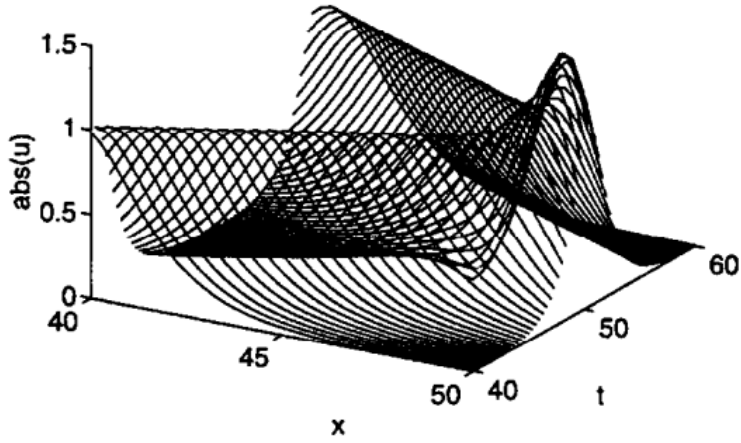
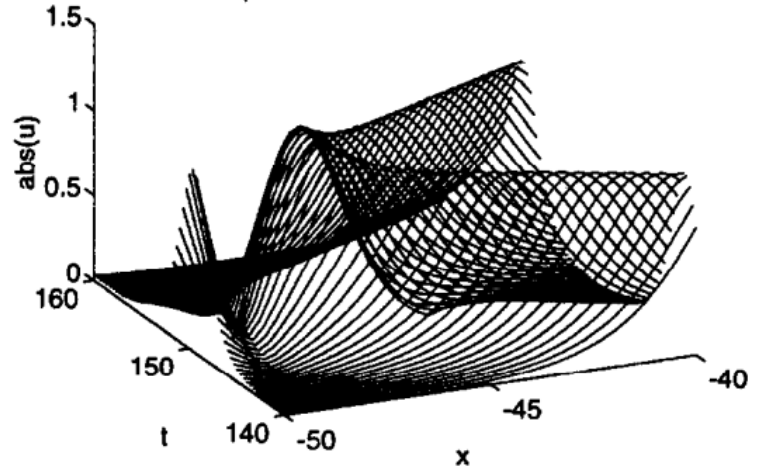


Figure 4. Amplitude, $|u|$, (top left), mass (top right), momentum (bottom left) and energy (bottom right) of a soliton colliding with a homogeneous Neumann boundary condition located at $x = 50$.

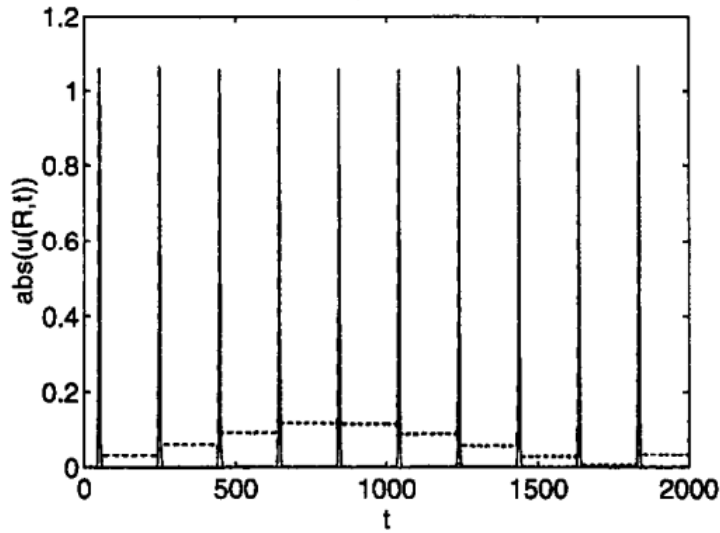
Robin right coll. out501



Robin left coll. out502



Bif. R=1,R=-1 out5.bif



Bif. R=1,R=-1 out5.bif

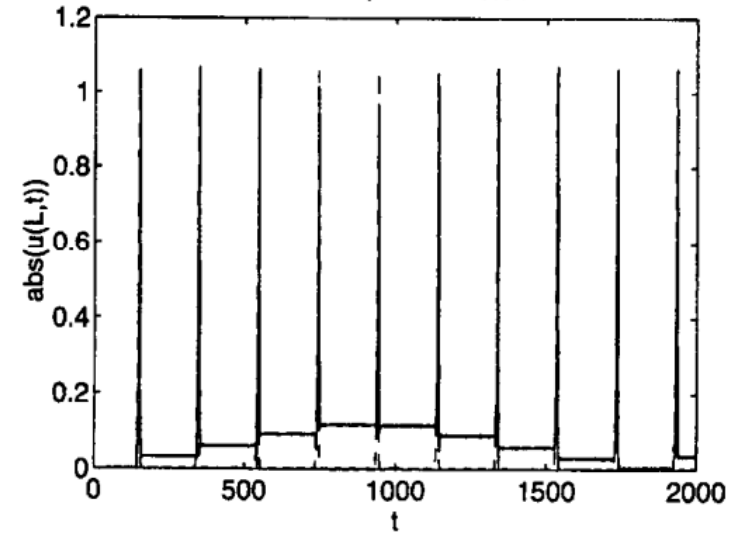


Figure 5. Amplitude, $|u|$, of a soliton colliding with the right (top left) and the left (top right) boundaries of a finite line subject to homogeneous Robin boundary conditions for $\gamma = 1$, and amplitude at the right (bottom left) and left (bottom right) boundaries for $\gamma = 1$ (continuous line) and -1 (dashed line).

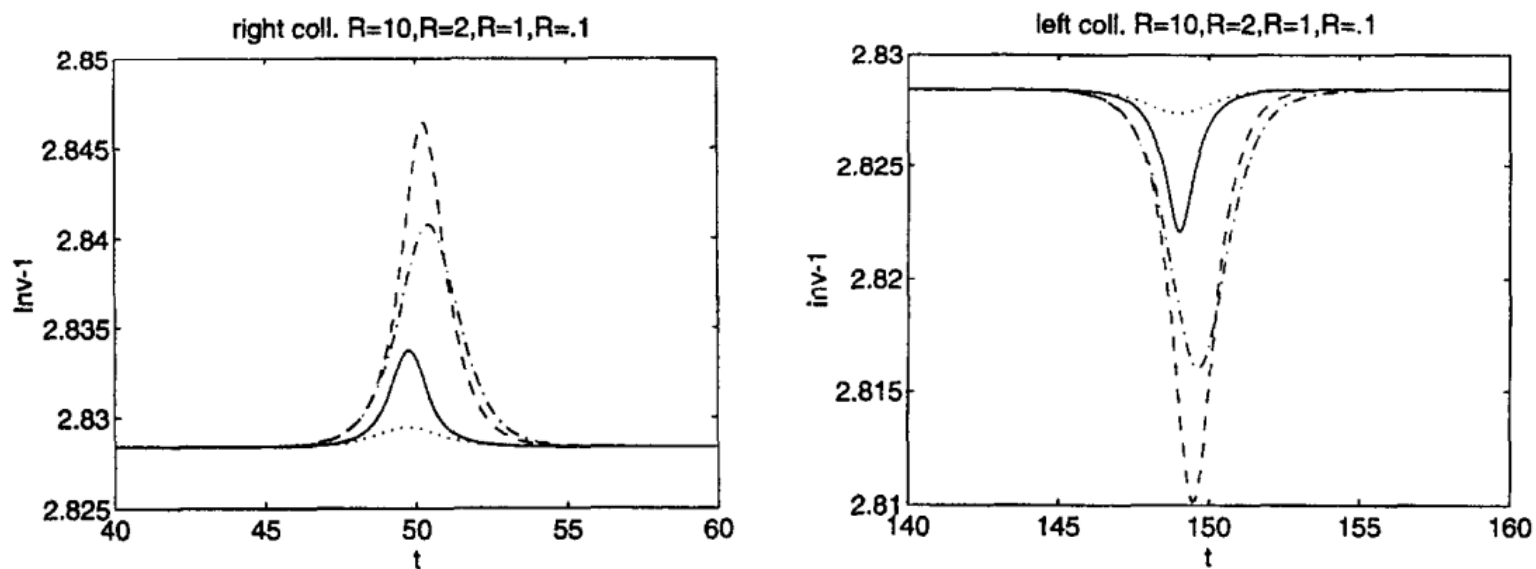


Figure 6. Mass of a soliton colliding with the right (left) and left (right) boundaries of a finite line subject to homogeneous Robin boundary conditions for $\gamma = 10$ (continuous line), 2 (dashed line), 1 (dotted-dashed line) and 0.1 (dotted line).

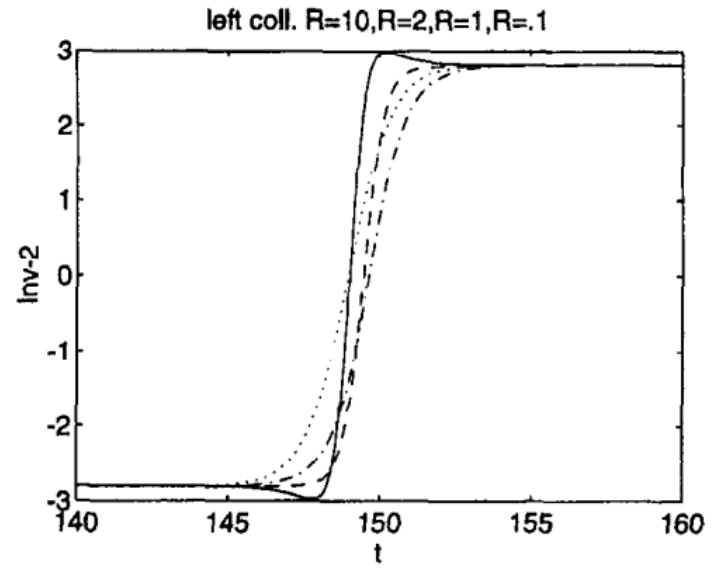
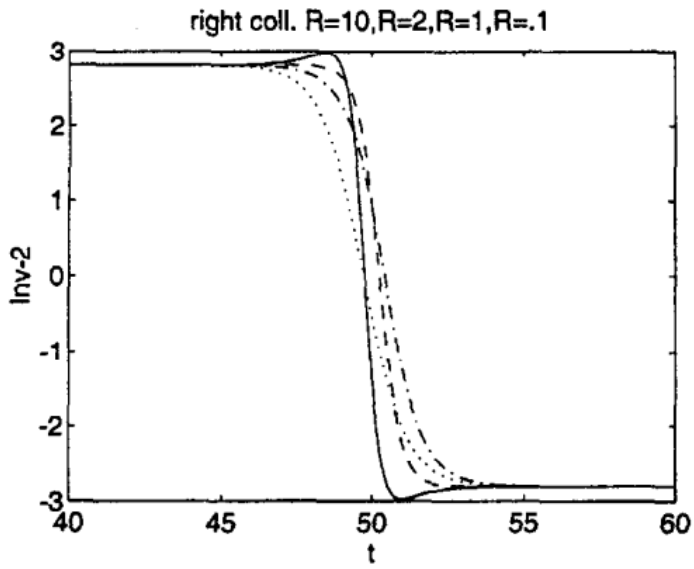


Figure 7. Momentum of a soliton colliding with the right (left) and left (right) boundaries of a finite line subject to homogeneous Robin boundary conditions for $\gamma = 10$ (continuous line), 2 (dashed line), 1 (dotted-dashed line) and 0.1 (dotted line).

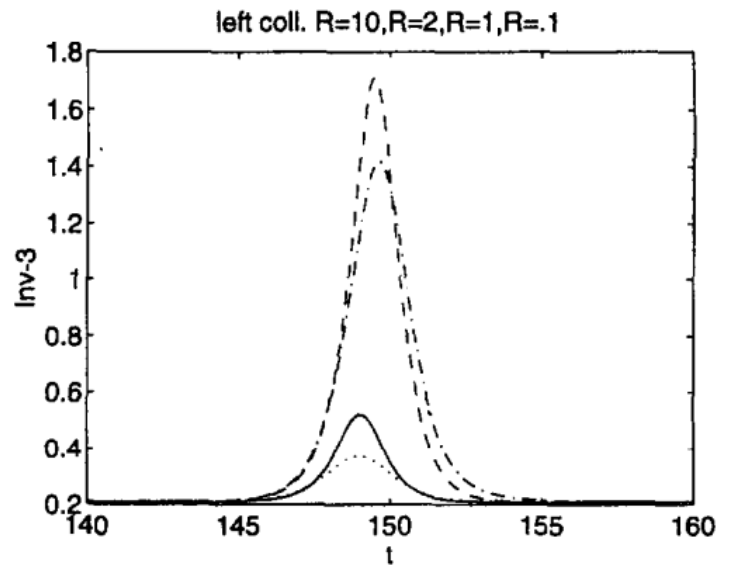
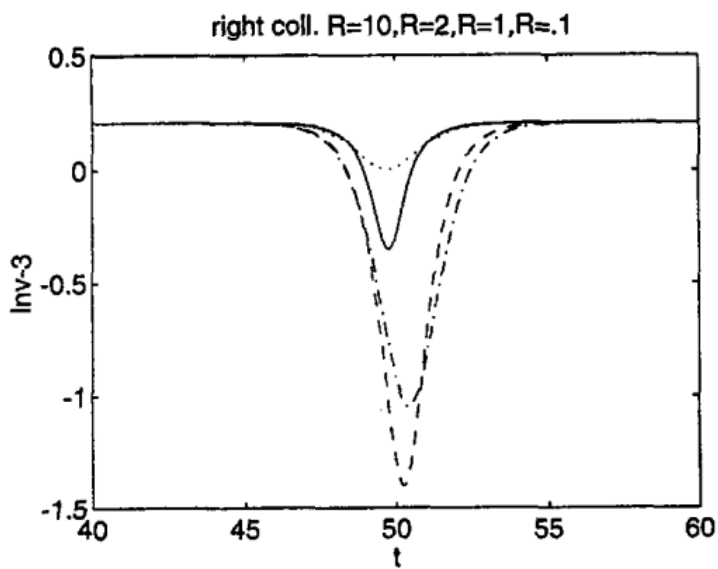


Figure 8. Energy of a soliton colliding with the right (left) and left (right) boundaries of a finite line subject to homogeneous Robin boundary conditions. ($\gamma = 10$ (continuous line), 2 (dashed line), 1 (dotted-dashed line), 0.1 (dotted line)).

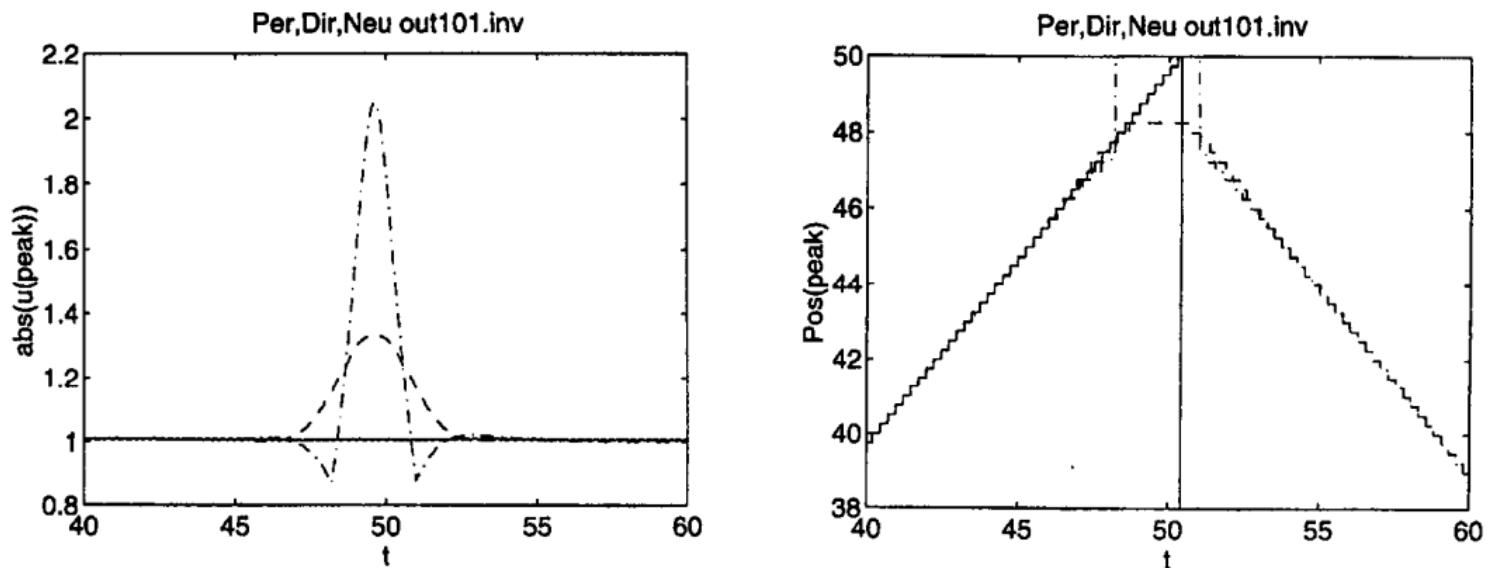


Figure 9. Maximum amplitude (left) and location of the maximum amplitude (right) of a soliton colliding with the right boundary of a finite line subject to periodic (continuous line), Dirichlet (dashed line) and Neumann (dotted-dashed line) boundary conditions.

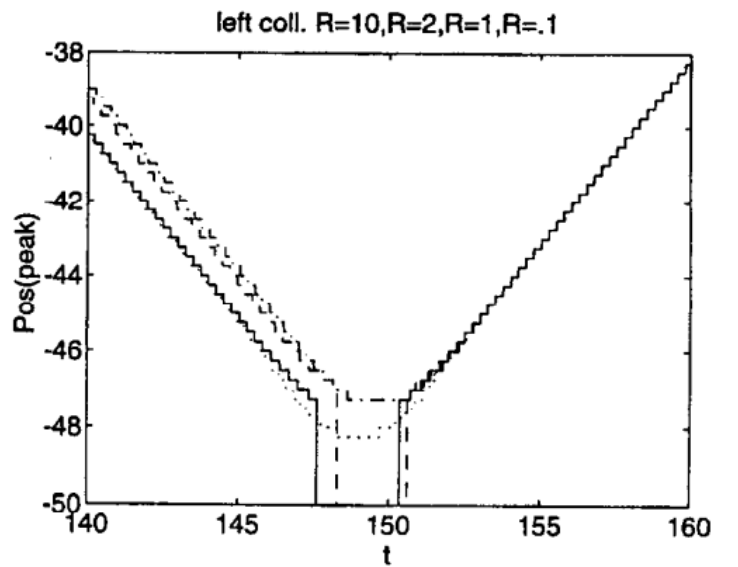
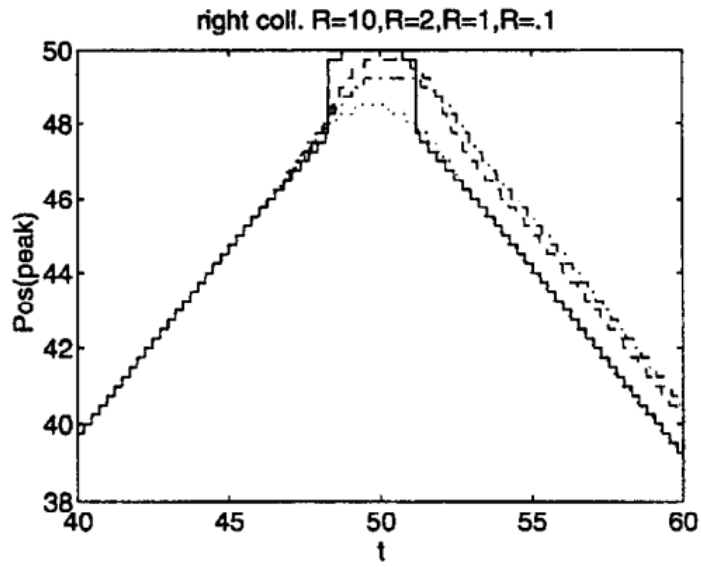
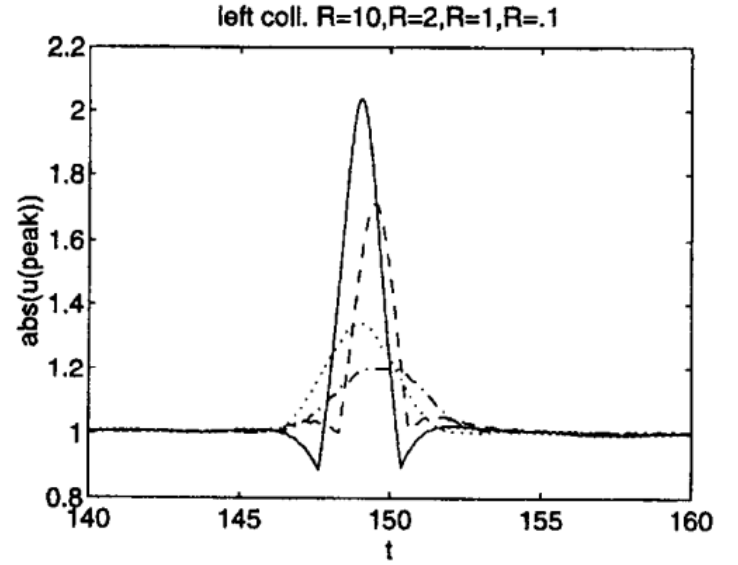
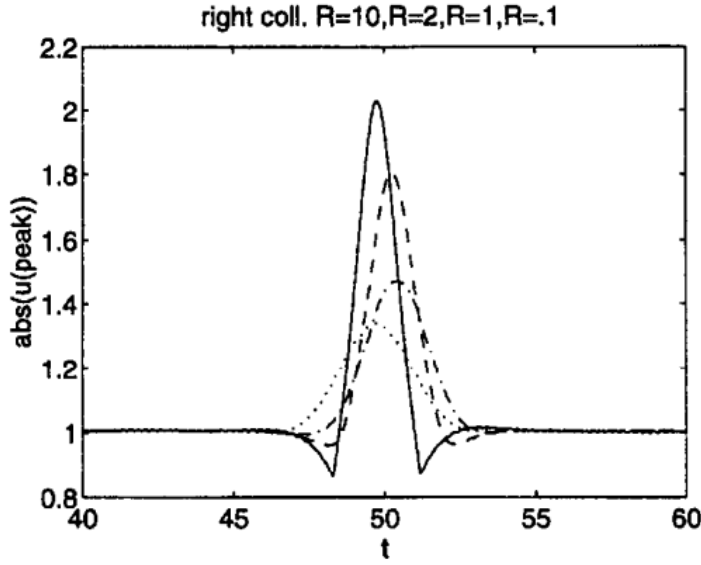


Figure 10. Maximum amplitude (top) and location of the maximum amplitude (bottom) of a soliton colliding with the right (left) and left (right) boundaries of a finite line subject to Robin boundary conditions. ($\gamma = 10$ (continuous line), 2 (dashed line), 1 (dotted-dashed line), 0.1 (dotted line)).

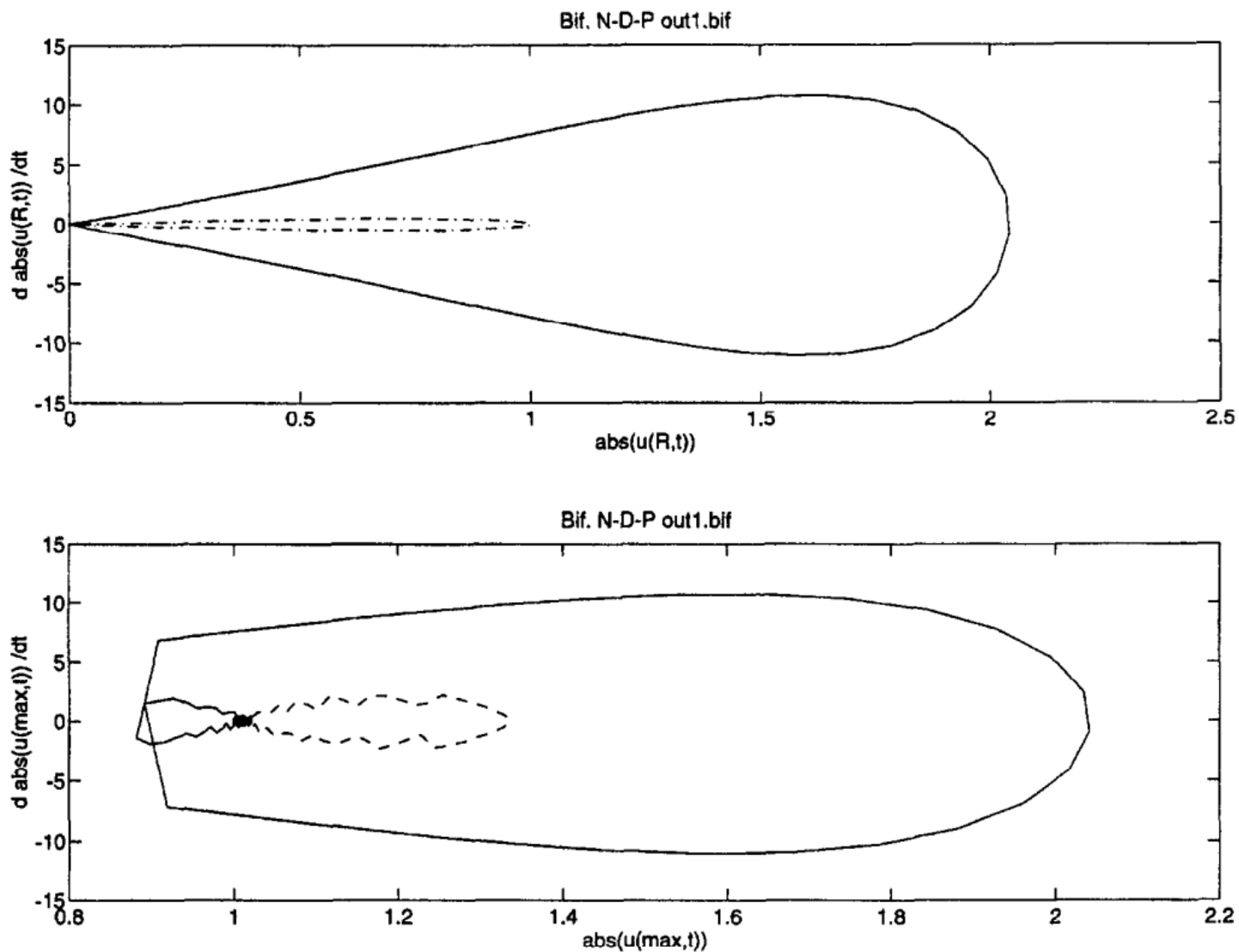


Figure 11. Phase diagrams of the amplitude at right boundary (top) and of the soliton's maximum amplitude (bottom) for the Neumann (continuous line), Dirichlet (dashed line) and periodic (dotted-dashed line) problems. Note that only one collision with the right boundary is presented, $L = 25$ and $\Delta x = 0.0625$.

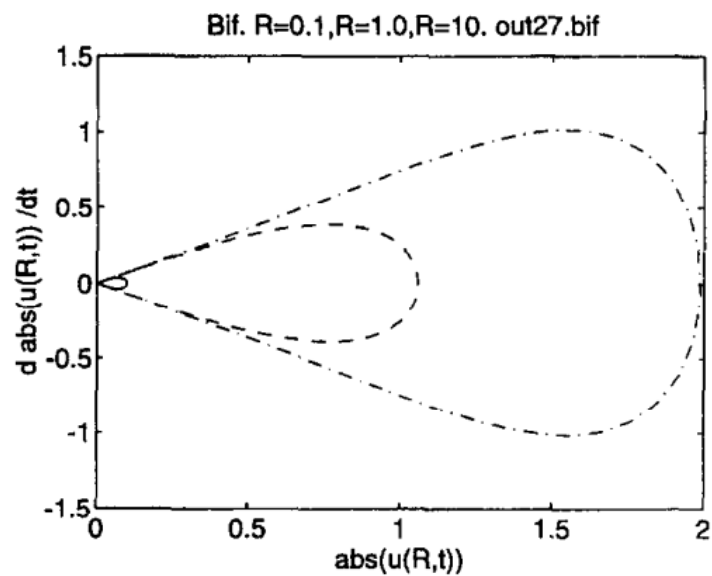
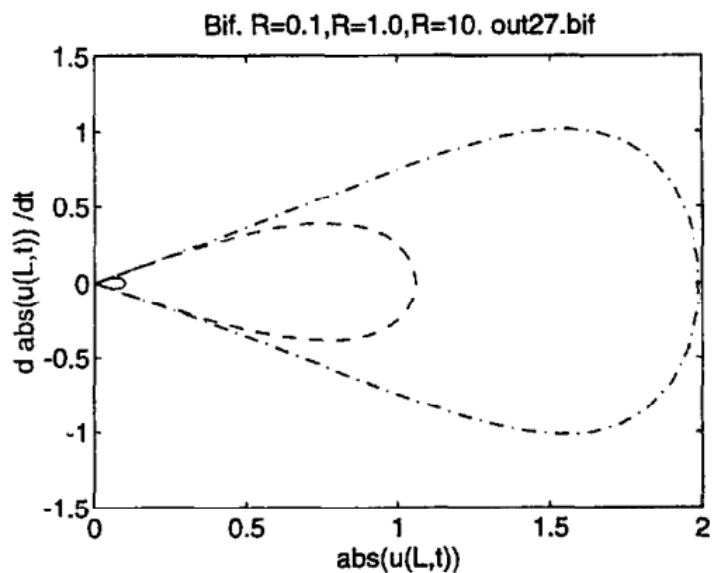


Figure 12. Phase diagrams of the amplitude at the left (left) and right (right) boundaries for the collision of a soliton with homogeneous Robin boundary conditions. Note that only one collision with each boundary is presented. ($L = 25$, $\Delta x = 0.0625$, and $\gamma = 0.1$ (continuous line), 1 (dashed line) and 10 (dotted-dashed line)).

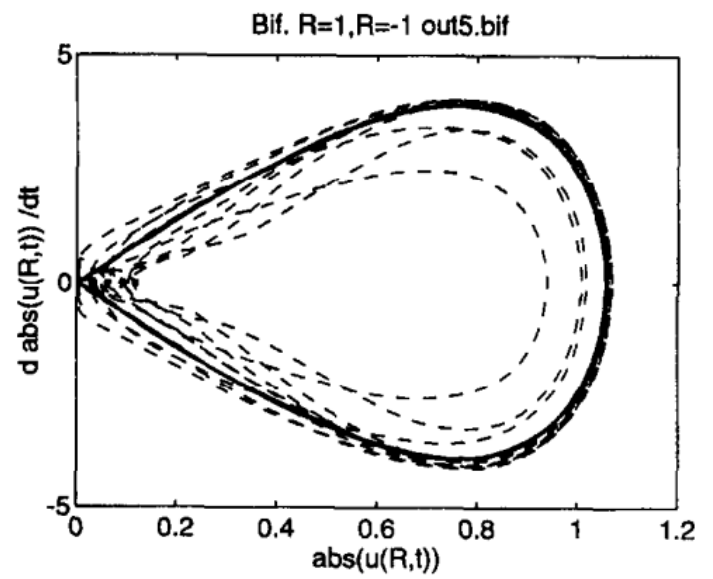
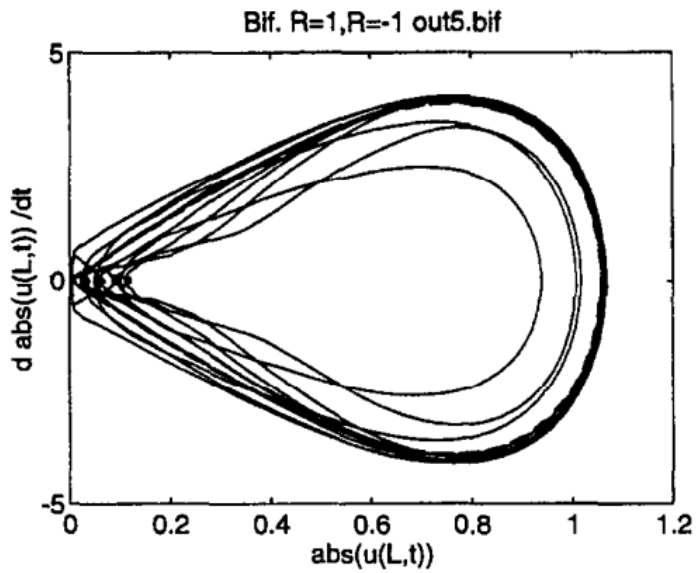


Figure 13. Phase diagrams of the amplitude at the left (left) and right (right) boundaries of a finite line subject to homogeneous Robin boundary conditions. Note that five collisions with each boundary are presented. ($\gamma = 1$ (continuous line) and -1 (dashed line)).

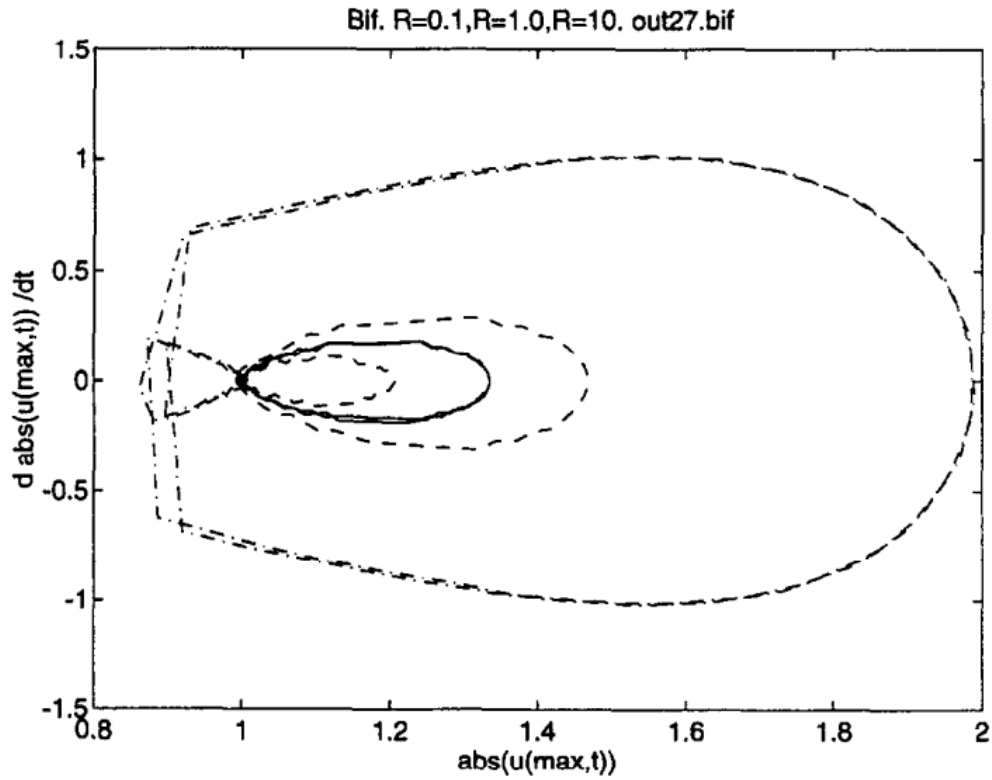


Figure 14. Phase diagram of the maximum amplitude for a Robin problem. Note that two collisions, one with each boundary, are presented, $L = 25$ and $\Delta x = 0.0625$. ($\gamma = 0.1$ (continuous line), 1 (dashed line) and 10 (dotted-dashed line)).

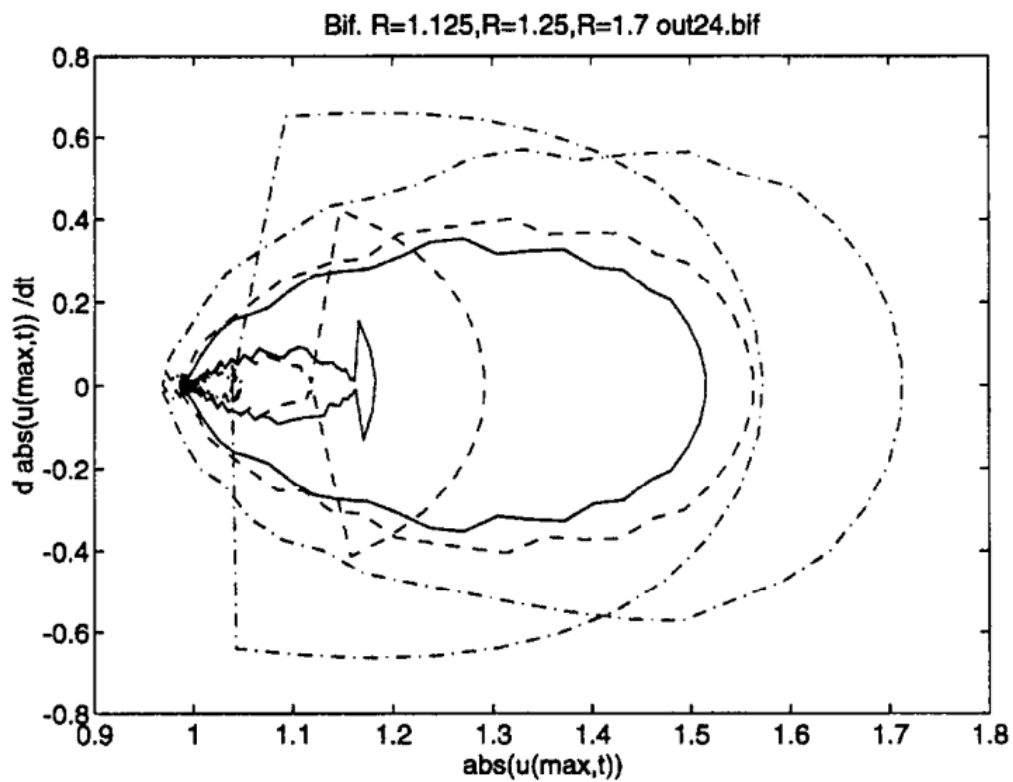


Figure 15. Phase diagram of the maximum amplitude for a Robin problem. Note that two collisions, one with each boundary, are presented, $L = 25$ and $\Delta x = 0.0625$. ($\gamma = 1.125$ (continuous line), 1.25 (dashed line) and 1.7 (dotted-dashed line)).

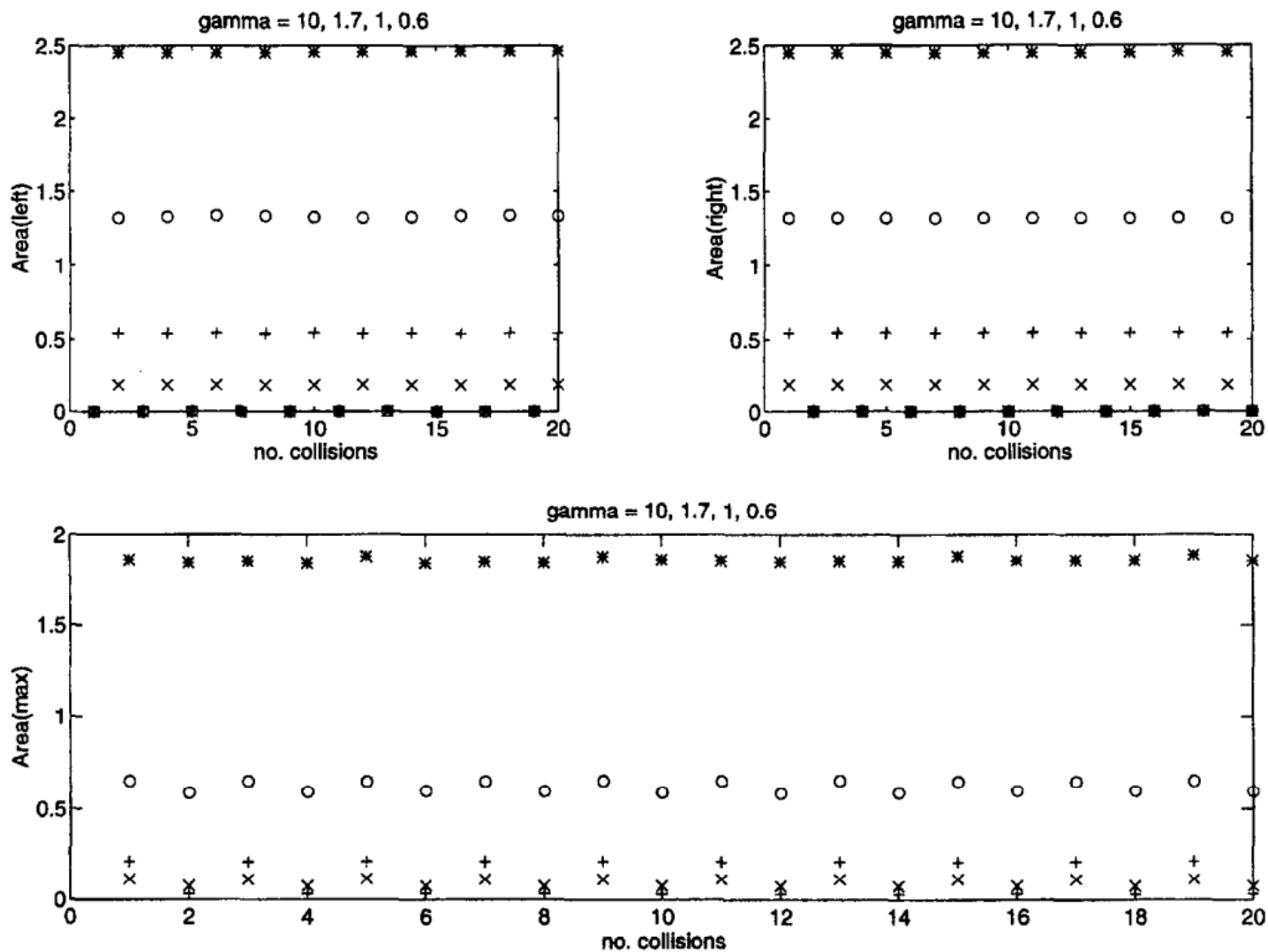


Figure 16. Areas of the phase diagrams corresponding to the amplitude at the left (top left) and right (top right) boundaries and to the soliton's maximum amplitude (bottom) as a function of the number of collisions for the Robin problem. Odd (even) collisions correspond to collisions of the soliton with the right (left) boundary. (The symbols *, o, +, and x correspond to $\gamma = 10, 1.7, 1$, and 0.6 , respectively).

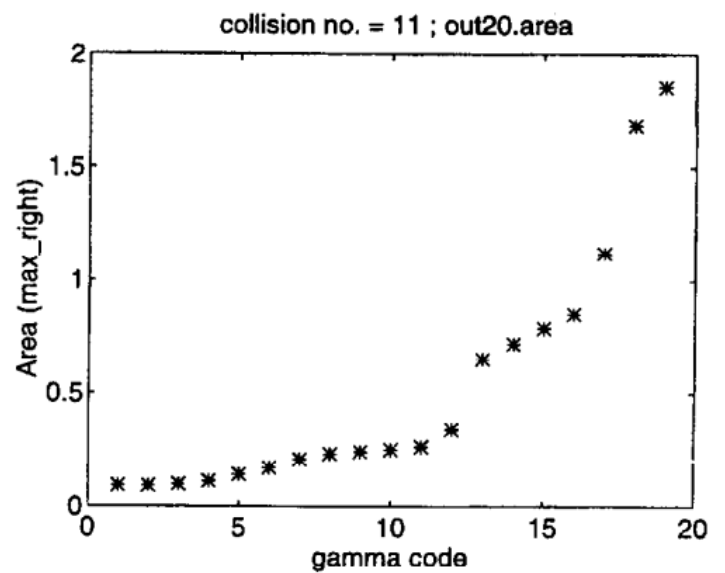
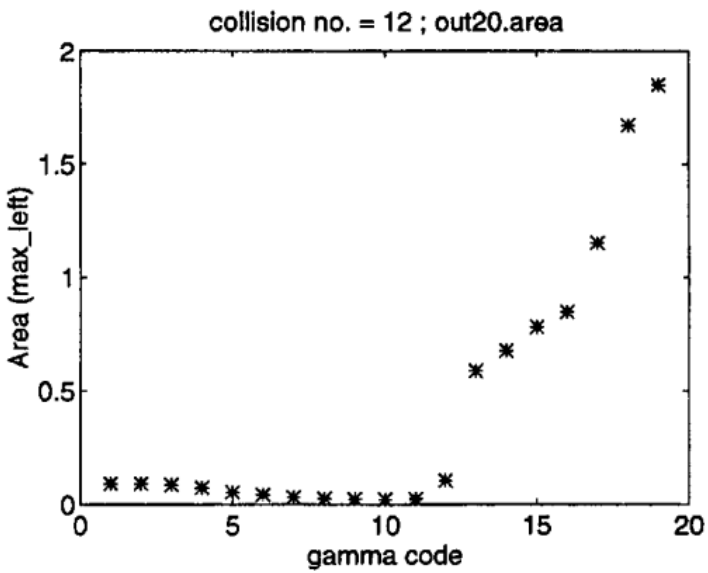
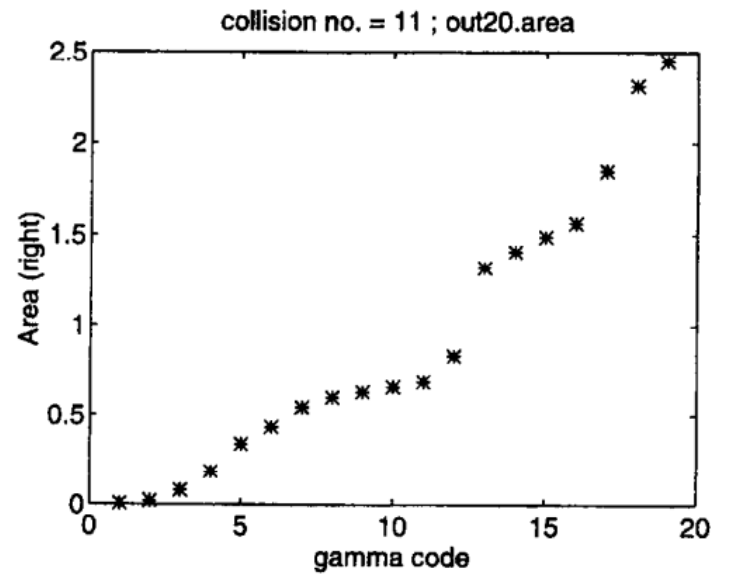
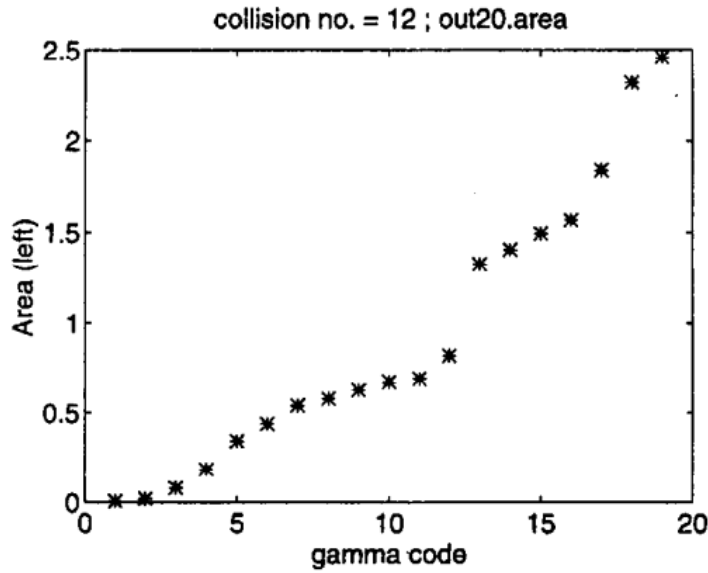


Figure 17. Areas of the phase diagrams corresponding to the amplitude at the left (top left) and right (top right) boundaries and to the maximum amplitude of the soliton for the sixth collision with the left (bottom left) and right (bottom right) boundaries as functions of γ . The values of $\gamma = 0.1, 0.2, 0.4, 0.6, 0.8, 0.9, 1.0, 1.05, 1.075, 1.1, 1.125, 1.25, 1.7, 1.8, 1.9, 2.0, 2.5, 5.0$ and 10 are represented by the natural numbers (gamma codes) from 1 to 19.